

structural details in this region are obscured by the temperature variation of the modulation wavelength and the incommensurability of the modulation and the lattice. However, for the commensurate $4.0 C_0$ structure obtained on warming through the 20- to 25°-K region, a satisfactory model has been obtained. In this model the basal-plane component assumes a spiral configuration and the c -axis component exhibits the variation: $\mu_0 = -\mu_3 = -\mu_4 = \mu_7 = 7.84 \mu_B$ and $\mu_1 = -\mu_2 = -\mu_5 = \mu_6 = 6.46 \mu_B$. In the 4.2- to 20°K region a ferromagnetic spiral structure is indicated. At 4.2°K, the spiral basal-plane component is $4.3 \mu_B$ while the ferromagnetic c -axis component is $7.9 \mu_B$. These yield a total ordered moment in good agreement with the $9 \mu_B$ expected for the Er^{3+} ion. The magnetic structures of the heavy rare earth metals have been discussed by several authors¹⁰⁻¹² who conclude that the rather startling variety of observed structures can be explained by the superimposed effects of an isotropic exchange interaction which imposes the moment modulation and a temperature-

dependent crystal-field anisotropy. The exchange interaction is assumed to be of the Rudermann-Kittel type which couples localized spins by polarization of the conduction electrons. It has been shown¹⁴⁻¹⁶ that this interaction, when applied to an hexagonal-close-packed array of localized spins in a system with three conduction electrons per atom, leads to a modulated-moment distribution with a modulation wavelength of about $3.6 C_0$ in remarkable agreement with these observations.

ACKNOWLEDGMENTS

We would like to express our appreciation to Professor S. Legvold and Professor F. H. Spedding of Iowa State University for the loan of the single-crystal samples used in this investigation.

¹⁴ E. J. Woll and S. J. Nettel, *Phys. Rev.* **123**, 796 (1961).

¹⁵ K. Yosida and A. Watabe, *Progr. Theoret. Phys. (Kyoto)* **28**, 361 (1962).

¹⁶ T. A. Kaplan and D. H. Lyons, *Phys. Rev.* **129**, 2072 (1963).

Theory of the Anisotropic Energy Gap in Superconducting Lead*†

ALAN J. BENNETT‡

Department of Physics and Institute for the Study of Metals, University of Chicago, Chicago, Illinois

(Received 15 July 1965)

The energy gap of a model anisotropic superconductor is considered. This model calculation forms the basis of a more realistic theoretical consideration of the energy gap of superconducting Pb, one in which the phonon density of states is the principal source of gap anisotropy. The effect of energy-band structure, important only near Brillouin-zone boundaries, is included as a perturbation. The phonon density of states is calculated from the experimental dispersion curves and singularities—present in the special density of states entering the superconductivity problem—are discussed. The phonon density of states and the isotropic gap solution obtained by previous workers are used to calculate the anisotropic part of the energy gap. The double gap, 2Δ , is found to have an absolute maximum of 2.86 meV in the $[100]$ direction, and an absolute minimum of 2.55 meV in the $[110]$ direction. Ten other maxima, minima, and saddle points are listed. The effect of the energy-gap anisotropy on electron-tunneling, electromagnetic-absorption, and acoustic-attenuation experiments is predicted.

I. INTRODUCTION

IN the original Bardeen-Cooper-Schrieffer¹ (BCS) formulation of the theory of superconductivity, a constant effective electron-electron interaction and spherical Fermi surface were assumed. The energy-gap equation, when solved under these assumptions, yielded an isotropic solution, i.e., one independent of crystallographic angle. These assumptions are, of course, too drastic, as the following experiments have shown:

- (1) electromagnetic absorption in Al,² Sn,³
- (2) acoustic attenuation in Sn,⁴ Zn,⁵
- (3) tunneling in Sn,⁶ Pb.^{7,8}

All these experiments indicate a range of energy gaps, i.e., an energy gap that varies with angle and may be different on different sheets of the Fermi surface.

² M. A. Biondi, M. P. Garfunkel, and W. A. Thompson, *Phys. Rev.* **136**, A1471 (1964).

³ P. L. Richards, *Phys. Rev. Letters* **7**, 412 (1961).

⁴ R. W. Morse, T. Olsen and J. D. Gavenda, *Phys. Rev. Letters* **3**, 15, 193 (1959); **3**, 193 (E) (1959).

⁵ H. V. Bohm and N. H. Horowitz, *Proceedings of the Eighth International Conference on Low Temperature Physics* (Butterworths Scientific Publications, Inc., Washington, 1963).

⁶ N. V. Zavaritskii, *Zh. Eksperim. i Teor. Fiz.* **43**, 1123 (1962) [English transl.: *Soviet Phys.—JETP* **16**, 793 (1962)].

⁷ P. Townsend and J. Sutton, *Phys. Rev.* **128**, 591 (1962).

⁸ G. I. Rochlin and D. H. Douglass, Jr., *Bull. Am. Phys. Soc.* **10**, 46 (1965).

* Supported in part by the National Aeronautics and Space Administration.

† Submitted in partial fulfillment of the requirements for the degree of Doctor of Philosophy at the University of Chicago.

‡ National Science Foundation predoctoral fellow.

¹ J. Bardeen, L. N. Cooper, and J. R. Schrieffer, *Phys. Rev.* **108**, 1175 (1957).

In an attempt to explain these results, Pokrovskii⁹ proposed a model in which he assumed an effective electron-electron interaction that depended only on the direction of the electron k vectors. Although he did not solve any specific model, he was able to obtain certain "universal" relations:

(1) The jump in the specific heat divided by the specific heat in the normal state at the critical temperature should be less than 1.4,

(2) the minimum value of the gap at $T=0$ divided by the critical temperature should be less than the BCS value.

These general relations agree in some cases¹⁰ with the experimental results for weak coupling superconductors. However, the relations are clearly violated in the case of lead and mercury. Since no attempt was made to calculate the form of the interaction, no predictions could be made as to the variation of the energy gap over the Fermi surface.

Pokrovskii and Ryvkin^{11,12} also investigated the effects of anisotropy on ultrasonic attenuation and electromagnetic absorption. While they were able to consider the general effect of an angular variation of the energy gap on these experimental observables, no quantitative predictions could be made in the absence of a detailed knowledge of $\Delta(\theta, \varphi)$ in an actual metal.

Experimental evidence indicates that, from the standpoint of its superconducting properties, the most anisotropic metal is probably tin, with indium and gallium also being highly anisotropic. However, since their electronic and lattice vibrational properties are not yet well known, we have chosen lead as the metal in which to compute the anisotropy. In lead, both the phonon spectrum¹³ and the band structure^{14,15} are known.

The primary purpose of this paper is to describe a calculation of $\Delta(\theta, \varphi)$ in lead. We use the results of the calculation to predict certain anomalies in experimentally observed quantities. As will be discussed below, we believe that the most important source of gap anisotropy is the phonon spectrum, and hence lead, a strong coupling superconductor, is well suited for investigation. In Sec. II, a consideration of a simple model of a superconductor helps to determine a suitable approach to a more realistic problem. With the use of a Green's function formalism (Sec. III) and the details of the phonon distribution (Sec. IV), we outline the actual

calculation of the gap anisotropy in Sec. V. Section VI consists of a description of the lead Fermi surface and its effects on the gap anisotropy. An analysis of the accuracy of our calculation is presented. In Sec. VII, we outline the basic approach used for comparing our results with experiments, in particular tunneling, infrared absorption, and acoustical attenuation.

II. SIMPLE-MODEL CALCULATION

In order to investigate the sources of anisotropy in the energy gap, we first consider a very simplified model of an anisotropic superconductor. Although, of course, no rigorous conclusions can be drawn from such a study, it is a useful guide to the more realistic calculation presented later. It is assumed that the energy-band structure of the material is ellipsoidal with complete azimuthal symmetry, i.e., the band energy ϵ is given by

$$\epsilon = \frac{\hbar^2 k^2}{2} \left(\frac{\cos^2 \theta}{m_1} + \frac{\sin^2 \theta}{m_2} \right), \quad (2.1)$$

where θ is the polar angle of the k vector. We further assume that the phonon dispersion relation is of the following form

$$\omega(\mathbf{q}) = \omega_0 + \omega_1 q_z^2, \quad (2.2)$$

where $q \cos \Theta = q_z$ is the projection of the phonon wave vector on the symmetry axis. This is a modified Einstein model, whose particular form is convenient for subsequent calculations.

We note here that Geilikman and Kresin¹⁶ have considered the gap anisotropy of a somewhat similar model, one with an ellipsoidal Fermi surface and an isotropic phonon distribution. Their source of gap anisotropy, the band-structure anisotropy acting through the matrix element for a single scattering of an electron by a phonon, leads to much smaller effects than those calculated in this section.

In the calculations, we use the following expansions:

$$\Delta_{\mathbf{k}} = \sum_n \Delta_n(\epsilon) P_n(\cos \theta), \quad n \text{ even}; \quad (2.3)$$

$$Q_{\mathbf{k}\mathbf{k}'} = Q(\epsilon, \epsilon', \theta, \theta') \\ = \sum_{l,m} Q_{lm}(\epsilon, \epsilon') P_l(\cos \theta) P_m(\cos \theta'), \quad (2.4)$$

where Δ is the energy gap and $Q = \rho V$ is the product of a density of states, defined below, and an interaction kernel. Here the P_n are Legendre polynomials, and symmetry considerations restrict n to even values. These functions satisfy a gap equation of the form

$$\Delta_{\mathbf{k}} = \sum_{\mathbf{k}'} \frac{V_{\mathbf{k}\mathbf{k}'} \Delta_{\mathbf{k}'}}{2(\epsilon_{\mathbf{k}'}^2 + \Delta_{\mathbf{k}'})^{1/2}}. \quad (2.5)$$

Because of the symmetry of Eqs. (2.1) and (2.2), the quantities in Eq. (2.5) are not functions of the azimuthal angle.

⁹ V. L. Pokrovskii, Zh. Eksperim. i Teor. Fiz. **40**, 641 (1961) [English transl.: Soviet Phys.—JETP **13**, 447 (1961)].

¹⁰ V. L. Pokrovskii and M. S. Ryvkin, Zh. Eksperim. i Teor. Fiz. **43**, 92 (1962) [English transl.: Soviet Phys.—JETP **16**, 67 (1963)].

¹¹ V. L. Pokrovskii, Zh. Eksperim. i Teor. Fiz. **40**, 898 (1961) [English transl.: Soviet Phys.—JETP **13**, 628 (1961)].

¹² V. L. Pokrovskii and M. S. Ryvkin, Zh. Eksperim. i Teor. Fiz. **40**, 1859 (1961) [English transl.: Soviet Phys.—JETP **13**, 1306 (1961)].

¹³ B. N. Brockhouse, T. Arase, G. Caglioti, K. R. Rao and A. D. B. Woods, Phys. Rev. **128**, 1099 (1962).

¹⁴ A. V. Gold, Phil. Trans. Roy. Soc. (London) **251**, 85 (1958).

¹⁵ J. R. Anderson and A. V. Gold, Phys. Rev. **139**, A1459 (1963).

¹⁶ B. T. Geilikman and V. Z. Kresin, Fiz. Tver. Tela **5**, 3549 (1963) [English transl.: Soviet Phys.—Solid State **5**, 2605 (1964)].

Thus Eq. (2.5) may be rewritten in the form

$$\Delta(\epsilon) = \int d\epsilon' \int d(\cos\theta') \frac{V(\epsilon, \theta, \epsilon', \theta') \Delta(\epsilon', \theta') \rho(\epsilon', \theta')}{2(\epsilon'^2 + \Delta^2(\epsilon', \theta'))^{1/2}}. \quad (2.6)$$

Using Eq. (2.1), we have replaced the variables k and k' by ϵ and ϵ' , respectively. $\rho(\epsilon', \theta')$ is the density of states such that

$$\rho(\epsilon', \theta') d(\cos\theta') d\epsilon' \quad (2.7)$$

is the number of states contained in k space between the surfaces ϵ' and $\epsilon' + d\epsilon'$, and θ' and $\theta' + d\theta'$. Thus

$$\begin{aligned} \rho(\epsilon', \theta') d\epsilon' d(\cos\theta') &= \frac{1}{2\pi^2} \int_{\theta'}^{\theta'+d\theta'} \int_b^a k'^2 dk' d(\cos\theta') \\ &= \frac{(2m_2)^{3/2} \epsilon'^{1/2} d\epsilon' d(\cos\theta')}{4\pi^2 \hbar^3 (1 + \beta \cos^2\theta')^{3/2}}, \end{aligned}$$

where

$$\begin{aligned} a &= \left[\frac{2(\epsilon' + d\epsilon')}{\hbar^2 \left(\frac{\cos^2\theta'}{m_1} + \frac{\sin^2\theta'}{m_2} \right)} \right]^{1/2}, \\ b &= \left[\frac{2\epsilon'}{\hbar^2 \left(\frac{\cos^2\theta'}{m_1} + \frac{\sin^2\theta'}{m_2} \right)} \right]^{1/2}, \\ \beta &= (m_2 - m_1)/m_1. \end{aligned} \quad (2.8)$$

We now assume a small anisotropy, i.e., $\beta \ll 1$. The use of a binomial expansion then gives

$$\rho(\epsilon', \theta') \cong (2m_2)^{3/2} (1 - \frac{3}{2}\beta \cos^2\theta') \epsilon'^{1/2} / 4\pi^2 \hbar^3. \quad (2.9)$$

In order to obtain an approximate expansion for $V_{\mathbf{k}\mathbf{k}'}$, we consider, as an example, the Bardeen-Pines interaction¹⁷⁻¹⁹

$$V_{\mathbf{k}\mathbf{k}'} = \frac{-2\hbar\omega_{\mathbf{k}-\mathbf{k}'} |g_{\mathbf{k}\mathbf{k}'\lambda}|^2}{(\epsilon_{\mathbf{k}} - \epsilon_{\mathbf{k}'})^2 - \hbar^2\omega_{\mathbf{k}-\mathbf{k}'}^2}. \quad (2.10)$$

Putting $\mathbf{k} - \mathbf{k}' = \mathbf{q}$, $\epsilon_{\mathbf{k}} - \epsilon_{\mathbf{k}'} = \delta\epsilon$, and using Eq. (2.2) for $\omega_{\mathbf{k}-\mathbf{k}'}$, we obtain, to lowest order in $\omega_1/\omega_0 = \alpha$,

$$V_{\mathbf{k}\mathbf{k}'} = \frac{2g^2(1 + \alpha q^2 \cos^2\Theta)}{\hbar\omega_0 [1 - (\delta\epsilon/\hbar\omega_0)^2 + 2\alpha q^2 \cos^2\Theta]}. \quad (2.11)$$

We have assumed here, as will be discussed in Sec. III, that $g_{\mathbf{k}\mathbf{k}'\lambda}$ is a constant g . In order to study this expres-

sion, we assume that

$$\frac{2\alpha q^2 \cos^2\Theta}{1 - (\delta\epsilon/\hbar\omega_0)^2} < 1. \quad (2.12)$$

This is certainly not true for all values of $\delta\epsilon$ that contribute to Eq. (2.5); it is, however, valid for those values for which the interaction is most attractive.

A further binomial expansion gives

$$V_{\mathbf{k}\mathbf{k}'} = \frac{2g^2(1 + \alpha \mathcal{R} q^2 \cos^2\Theta)}{\hbar\omega_0 [1 - (\delta\epsilon/\hbar\omega_0)^2]}, \quad (2.13)$$

where

$$\mathcal{R} = 1 - \frac{2}{1 - (\delta\epsilon/\hbar\omega_0)^2}.$$

If

- (1) use is made of Eqs. (2.13), (2.9), and (2.5),
- (2) terms of order α^2 , β^2 , $\alpha\beta$ or higher are neglected,
- (3) orthogonality properties of Legendre polynomials are taken in account,
- (4) only terms of the second order and lower in the Legendre polynomial expansions are used,
- (5) we note that to lowest order the $\Delta(\epsilon', \theta')$ appearing under the square root in the denominator of Eq. (2.5) may be replaced by $\Delta_0(\epsilon')$,

then Eq. (2.5) reduces to,

$$\begin{aligned} \Delta(\epsilon, \theta) &\cong \Delta_0(\epsilon) + \Delta_2(\epsilon) P_2(\cos\theta) \\ &= \int d\epsilon' \frac{[Q_{00}(\epsilon, \epsilon') \Delta_0(\epsilon') + Q_{02}(\epsilon, \epsilon') \Delta_2(\epsilon')]}{(\epsilon'^2 + \Delta_0^2(\epsilon'))^{1/2}} \\ &\quad + \left[\int d\epsilon' \frac{Q_{20}(\epsilon, \epsilon') \Delta_0(\epsilon')}{(\epsilon'^2 + \Delta_0^2(\epsilon'))^{1/2}} \right] P_2(\cos\theta), \end{aligned} \quad (2.14)$$

where

$$Q_{20} = \alpha A, \quad (2.15)$$

$$Q_{02} = \alpha A - \beta B, \quad (2.16)$$

and Q_{00} is, of course, independent of α and β . A and B are quantities independent of the anisotropy parameters.

Comparison of the coefficients of the polynomials gives to lowest order

$$\Delta_0(\epsilon) = \int d\epsilon' \frac{Q_{00}(\epsilon, \epsilon') \Delta_0(\epsilon')}{(\epsilon'^2 + \Delta_0^2(\epsilon'))^{1/2}}, \quad (2.17)$$

which is the ordinary BCS-type equation, and

$$\Delta_2(\epsilon) = \int d\epsilon' \frac{Q_{20}(\epsilon, \epsilon') \Delta_0(\epsilon')}{(\epsilon'^2 + \Delta_0^2(\epsilon'))^{1/2}}. \quad (2.18)$$

We note that in this approximation, $\Delta_2(\epsilon)$ is not a function of β , the energy-band anisotropy. It is, however, directly proportional to the phonon anisotropy parameter α . This observation is of relevance for the more

¹⁷ J. Bardeen and D. Pines, Phys. Rev. **99**, 1140 (1955).

¹⁸ G. M. Eliashberg, Zh. Eksperim. i Teor. Fiz. **38**, 966 (1960) [English transl.: Soviet Phys.—JETP **11**, 696 (1960)].

¹⁹ The Eliashberg interaction is, of course, more accurate than Bardeen-Pines interaction, but for the purposes of this discussion they are equally valid and the latter is simpler in form.

realistic calculation of the gap anisotropy to be discussed below.

The effects of the electron band structure must, of course, be considered, especially near the Brillouin-zone boundaries, where the effects of the crystal potential are strongest and seriously influence the connectivity of the Fermi surface. Quantitatively, this effect is only of importance in about 10% of the Brillouin zone. It is considered as a perturbation (in the sense of degenerate perturbation theory) after the basic phonon-induced anisotropy is calculated.

If we make a BCS-like assumption, i.e., assume that Q_{02} and Q_{00} are constants in a small energy interval about the Fermi energy and zero outside it, we find that

$$\Delta_2 = c\Delta_0, \quad (2.19)$$

where c is a constant.

We may see from Eq. (2.18) that it is possible to calculate the anisotropic part of the energy gap by reducing the integral equation to a simple integral. In a later section, we use this same type of reduction to solve for the gap anisotropy in lead.

We now consider, in a more general fashion, the iteration scheme which will be used. If we write

$$\Delta(\epsilon, \theta, \varphi) = \Delta_0(\epsilon) + \Delta_1(\epsilon, \theta, \varphi), \quad (2.20)$$

where $\Delta_1 \ll \Delta_0$, and

$$Q(\epsilon, \theta, \varphi, \epsilon', \theta', \varphi') = Q_0(\epsilon, \epsilon') + Q_1(\epsilon, \theta, \varphi, \epsilon', \theta', \varphi'), \quad (2.21)$$

where $Q_1 \ll Q_0$, then these functions satisfy the following equations:

$$\Delta = \iiint d\epsilon' d(\cos\theta') d\varphi' \frac{Q\Delta}{E}, \quad (2.22)$$

and

$$\Delta_0 = \iiint d\epsilon' d(\cos\theta') d\varphi' \frac{Q_0\Delta_0}{E_0}, \quad (2.23)$$

where

$$E_0 = (\epsilon'^2 + \Delta_0^2(\epsilon'))^{1/2}, \quad (2.24)$$

$$E = (\epsilon'^2 + \Delta^2(\epsilon', \theta', \varphi'))^{1/2}. \quad (2.25)$$

Substituting Eqs. (2.20) and (2.21) in (2.22), we have

$$\Delta_0 + \Delta_1 = \iiint d\epsilon' d(\cos\theta') d\varphi' \times \frac{(Q_0\Delta_0 + Q_0\Delta_1 + Q_1\Delta_0 + Q_1\Delta_1)}{E}, \quad (2.26)$$

but

$$\frac{1}{E} = \frac{1}{E_0} + \frac{E_0 - E}{EE_0}, \quad (2.27)$$

hence

$$\Delta_1 = \iiint d\epsilon' d(\cos\theta') d\varphi' \times \left[\frac{Q_0\Delta_0(E_0 - E)}{EE_0} + \frac{Q_0\Delta_1 + Q_1\Delta_0 + Q_1\Delta_1}{E} \right]. \quad (2.28)$$

In order to investigate the relative importance of the terms on the right-hand side of this equation, we allow the parameter describing the anisotropy to approach zero. Then, if we choose the physically meaningful solution Δ_1 , i.e., the one that approaches zero with the anisotropy parameter, and note that

(1) the term in $Q_1\Delta_1$ is second order and may be neglected,

(2) $(E_0 - E)/EE_0$ can be expanded in powers of $2\Delta_0\Delta_1/(\epsilon^2 + \Delta_0^2)$,

we find to lowest order in the anisotropy that

$$\Delta_1 = \iiint d\epsilon' d(\cos\theta') d\varphi' \times \left[\frac{-Q_0\Delta_0^2\Delta_1/(\epsilon'^2 + \Delta_0^2) + Q_0\Delta_1 + Q_1\Delta_0}{E_0} \right]. \quad (2.29)$$

In accord with the normal iterative method of solving an integral equation, we let $\Delta_1 = 0$ under the integral and integrate

$$\Delta_1 = \iiint d\epsilon' d(\cos\theta') d\varphi' \frac{Q_1\Delta_0}{E_0}. \quad (2.30)$$

We may then use this result in Eq. (2.29) for higher approximations. In practice, we shall stop after one iteration, since the numerical integrals which must be performed for greater accuracy are very involved. We also note that if Δ_1 contains no angle-independent part, it can be expanded in spherical harmonics $Y_l^m(\cos\theta, \varphi)$ with $l > 0$. Since for $l > 0$

$$\iiint Y_l^m(\cos\theta, \varphi) d(\cos\theta) d\varphi = 0, \quad (2.31)$$

and Q_0 , E_0 , and Δ_0 are independent of angle, only the last term in Eq. (2.29) contributes. In addition, the angular integration in Eq. (2.30) ensures that only the part of Q_1 which is independent of θ' and φ' gives a non-zero contribution.

III. THE GAP EQUATION FOR STRONG-COUPLING SUPERCONDUCTORS

We have seen in the last section that in order to calculate the anisotropic part of the energy gap, we must have an accurate solution for $\Delta_0(\epsilon)$, the isotropic part of the gap. It is well known that some superconductors, e.g., lead and mercury,²⁰ do not satisfy the conditions of the original BCS model in which the coupling parameter $N(0)V$ is small. For these strong-coupling superconductors, the electron-phonon interaction is so strong that the quasiparticles are no longer well defined over

²⁰ J. C. Swihart, D. J. Scalapino, and Y. Wada, Phys. Rev. Letters **14**, 106 (1965).

the entire energy spectrum. In the remainder of this section, we shall briefly outline the Nambu²¹-Gorkov^{22,23} formalism, which allows for the inclusion of damping and retardation effects, and obtain the equations needed to calculate the anisotropy.

We start by defining the Green's functions for electrons and phonons and considering the electron-phonon coupling. The one-electron Green's function for the noninteracting system is given in the momentum representation by

$$\mathbf{G}_0(\mathbf{p}, p_0) = \frac{p_0 \mathbf{1} + \epsilon_p \boldsymbol{\tau}_3}{p_0^2 - \epsilon_p^2 + i\delta}, \quad (3.1)$$

where \mathbf{p} and p_0 are the quasiparticle's momentum and energy, ϵ_p is the band energy measured from the Fermi level, and $\mathbf{1}$, $\boldsymbol{\tau}$ are the usual unit and Pauli spin matrices. The matrix form of Dyson's equation for the Green's function of the interacting electron is

$$\mathbf{G}^{-1}(\mathbf{p}, p_0) = \mathbf{G}_0^{-1}(\mathbf{p}, p_0) - \boldsymbol{\Sigma}(\mathbf{p}, p_0), \quad (3.2)$$

where $\boldsymbol{\Sigma}$, the irreducible self-energy of the superconducting system, is of the general form

$$\boldsymbol{\Sigma}(\mathbf{p}, p_0) = [1 - Z(\mathbf{p}, p_0)] p_0 \mathbf{1} + \chi(\mathbf{p}, p_0) \boldsymbol{\tau}_3 + \phi(\mathbf{p}, p_0) \boldsymbol{\tau}_1. \quad (3.3)$$

This formula should be considered the defining relation for the functions Z , χ , and ϕ . We note that

$$\Delta(\mathbf{p}, p_0) \equiv \phi(\mathbf{p}, p_0) / Z(\mathbf{p}, p_0) \quad (3.4)$$

can be shown to correspond to the BCS energy gap, e.g.,

$$\Delta(\mathbf{p}_F, \Delta_{\text{BCS}}) = \Delta_{\text{BCS}}. \quad (3.5)$$

$Z(\mathbf{p}, p_0)$ is a renormalization factor that enters into a calculation of the effective mass, and $\chi(\mathbf{p}, p_0)$ changes the effective mass and chemical potential, but does not enter the superconductivity problem in an essential way. Using Eqs. (3.1), (3.2), and (3.3), one finds

$$\mathbf{G}(\mathbf{p}, p_0) = \frac{Z(\mathbf{p}, p_0) p_0 \mathbf{1} + \epsilon_p \boldsymbol{\tau}_3 + \phi(\mathbf{p}, p_0) \boldsymbol{\tau}_1}{[Z(\mathbf{p}, p_0) p_0]^2 - E^2(\mathbf{p}, p_0) + i\delta}, \quad (3.6)$$

where

$$E^2(\mathbf{p}, p_0) = \epsilon_p^2 + \phi^2(\mathbf{p}, p_0). \quad (3.7)$$

The one-phonon Green's function, expressed in terms of a spectral representation, is given in momentum

$$\Delta(\mathbf{p}, p_0) = \frac{N(0)}{Z(\mathbf{p}, p_0)} \int_{\Delta_{\text{BCS}}}^{\omega_c} d p_0' \operatorname{Re} \left[\frac{\Delta(p_0')}{(p_0'^2 - \Delta^2(p_0'))^{1/2}} \right] [K_{+}^{\text{phonon}}(p_0, p_0') - U_c], \quad (3.11)$$

$$[1 - Z(\mathbf{p}, p_0)] p_0 = N(0) \int_{\Delta_{\text{BCS}}}^{\omega_c} d p_0' \operatorname{Re} \left[\frac{p_0'}{(p_0'^2 - \Delta^2(p_0'))^{1/2}} \right] K_{-}^{\text{phonon}}(p_0, p_0'), \quad (3.12)$$

²¹ Y. Nambu, Phys. Rev. **117**, 648 (1960).

²² L. P. Gorkov, Zh. Eksperim. i Teor. Fiz. **34**, 735 (1958) [English transl.: Soviet Phys.—JETP **7**, 505 (1958)].

²³ This description is based on the presentation of J. R. Schrieffer's *Theory of Superconductivity* (W. A. Benjamin, Inc., New York 1964).

²⁴ J. M. Ziman, *Electrons and Phonons* (Clarendon Press, Oxford, 1960), Chap. V.

²⁵ J. R. Schrieffer, D. J. Scalapino, and J. W. Wilkins, Phys. Rev. Letters **10**, 336 (1963).

space by

$$D_\lambda(\mathbf{q}, q_0) = \int_0^\infty \frac{B_\lambda(\mathbf{q}, \omega) 2\omega d\omega}{q_0^2 - \omega^2 + i\delta}, \quad (3.8)$$

where λ designates the polarization mode and $B_\lambda(\mathbf{q}, \omega)$ is the so-called weight function. For bare phonons, it reduces to

$$B_\lambda(\mathbf{q}, \omega) = \delta(\omega - \Omega_{\mathbf{q}\lambda}), \quad (3.9)$$

where $\Omega_{\mathbf{q}\lambda}$ is the energy of a bare phonon of wave vector \mathbf{q} and polarization λ .

One further quantity needed in the calculation is the matrix element $g_{\mathbf{p}\mathbf{p}'\lambda}$ for the electron-phonon interaction involving electronic states of momentum \mathbf{p} and \mathbf{p}' and a phonon of momentum $\mathbf{p} - \mathbf{p}'$ and polarization λ . The form²⁴ of the actual $g_{\mathbf{p}\mathbf{p}'\lambda}$ may be quite complicated.

Since a reliable calculation of the anisotropy of $g_{\mathbf{p}\mathbf{p}'\lambda}$ has not as yet been performed, we will not attempt to obtain the anisotropic part of the energy gap due to the electron-phonon interaction. As will be shown below, the effect of the anisotropy of $g_{\mathbf{p}\mathbf{p}'\lambda}$ is an additive one, i.e., one that may be added to that part caused by the phonon density of states and the band structure.

The self-energy may now be expressed in terms of the electron and phonon Green's functions which are themselves functions of the self-energy. This procedure, when carried out to lowest order in the phonon and Coulomb contributions, results in the following integral equation

$$\boldsymbol{\Sigma}(\mathbf{p}, p_0) = i \int \boldsymbol{\tau}_3 \mathbf{G}(\mathbf{p}', p_0') \boldsymbol{\tau}_3 [\sum_\lambda \{g_{\mathbf{p}\mathbf{p}'\lambda}\}^2 \times D_\lambda(\mathbf{p} - \mathbf{p}', p_0 - p_0') + V_c(\mathbf{p} - \mathbf{p}')] \frac{d^4 p'}{(2\pi)^4}, \quad (3.10)$$

where V_c is considered a statically screened Coulomb interaction. The terms in the square brackets correspond, in the BCS theory, to the instantaneous interaction $V_{\mathbf{p}\mathbf{p}'}$. In the isotropic case considered by Schrieffer, Scalapino, and Wilkins²⁵ (SSW), it can be shown that on the right-hand side of Eq. (3.10), i.e., under the integral sign, $\boldsymbol{\Sigma}(\mathbf{p}', p_0')$ may be considered a function of p_0' only. After some mathematical manipulation, including a transformation to the coordinate system shown in Fig. 1, and the introduction of a pseudopotential U_c to represent the Coulomb contribution, the integral equations determining Δ and Z are obtained:

where

$$K_{\pm}^{\text{phonon}}(p_0, p_0') = \int_0^{\infty} d\omega \sum_{\lambda} F^{\lambda}(\omega) \left[\frac{1}{p_0' + p_0 + \omega - i\delta} \pm \frac{1}{p_0' - p_0 + \omega - i\delta} \right]. \quad (3.13)$$

Here $N(0)$ is the density of electronic states at the Fermi energy, ω_c is a cutoff of the order of the Debye energy, which (as will be discussed below), for \mathbf{p} close to the Fermi surface, restricts \mathbf{p}' to be also close to the Fermi surface.

$F^{\lambda}(\omega)$ is essentially an effective density of phonon states. It gives the number of phonons of energy between ω and $\omega + d\omega$ and polarization λ whose wave vectors \mathbf{q} connect an electronic state of fixed vector \mathbf{p} on (or close to) the Fermi surface and other electronic states $\mathbf{p}' = \mathbf{p} + \mathbf{q}$ near the surface. In the isotropic case, $F^{\lambda}(\omega)$ is independent of the direction of \mathbf{p} , and because of the form of Eq. (3.10), it is essentially independent of its magnitude.²³ Thus Δ and Z given by Eqs. (3.11) and (3.12) depend only on p_0 . When no anisotropy is present, $F^{\lambda}(\omega)$ may be expressed as

$$N(0)F^{\lambda}(\omega) \propto \int_0^{2p_F} q dq \int_0^{2\pi} d\varphi |g_{q\lambda}|^2 B_{\lambda}(q, \omega), \quad (3.14)$$

where p_F is the Fermi momentum.

In order to obtain a numerical solution to these equations for isotropic lead, SSW assumed that

$$N(0)F^{\lambda}(\omega) = \frac{\omega_{\lambda}\omega_2^{\lambda}\pi}{(\omega - \omega_1^{\lambda})^2 + (\omega_2^{\lambda})^2}, \quad (3.15)$$

i.e., $F^{\lambda}(\omega)$ was given by a Lorentzian; they adjusted the parameters of the Lorentzians so as to reproduce roughly the phonon density of states obtained from experiment.¹³ It was assumed that the constant ω_{λ} was the same for all modes and it was chosen so that $\Delta(\Delta_{\text{BCS}})$ equaled 1.34 meV—the value observed in dirty-lead samples. A successful test of this calculation was its ability to reproduce the tunneling data of Rowell, Anderson, and Thomas.²⁶

We follow the general approach developed in the preceding section, and assume that in a first-order calculation of the gap anisotropy it is not only possible to ignore the variation of Σ with p but also its variation with angle, when Σ appears on the right-hand side of Eqs.

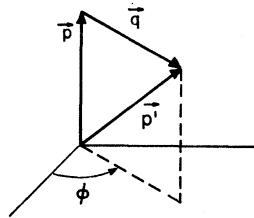


FIG. 1. The coordinate system used in obtaining the gap equations (3.11) through (3.14).

(3.11) and (3.12). That is, when $Z(\mathbf{p}, p_0)$ and $\Delta(\mathbf{p}, p_0)$ appear under the integral sign, they may be considered functions of p_0 only. Using our assumption that the effects of energy-band anisotropy may be added later, we need now only consider anisotropy in $K_{\pm}^{\text{phonon}}(p_0, p_0')$. The only change in Eqs. (3.11) and (3.12) is that now $F^{\lambda}(\omega)$ must be replaced by $F^{\lambda}(\omega, \theta, \varphi)$, where the θ and φ indicate that the effective density of states involved consists of those phonons whose wave vectors \mathbf{q} connect the electronic state (p, θ, φ) on (or close to) the Fermi surface with other electronic states also on (or close to) the Fermi surface (see Fig. 2).

We again emphasize that we are ignoring the effect of the anisotropic part of the electron-phonon coupling. Because of the linear way in which the anisotropic part of g would enter Eq. (3.14), and because of our approximation scheme, this omission can be readily corrected, when more becomes known about the coupling anisotropy.

The upper integration cutoff in Eqs. (3.11) and (3.12) is determined by noting that the phonon propagator (3.8) varies as $(p_0 - p_0')^{-2}$ for $|p_0 - p_0'| > \omega_{p-p'}$. Hence the major contribution to the integrals comes from values of $|p_0 - p_0'|$ less than ω_c , a cutoff somewhat larger than the Debye frequency, but much smaller than the Fermi energy. The particular form of \mathbf{G} , Eq. (3.6), ensures that the electron energies ϵ_p , which are responsible for the dominant contribution to the integrals are also less than ω_c , and are thus confined to a small region in the vicinity of the Fermi surface. For the purpose of calculating the phonon density of states $F^{\lambda}(\omega, \theta, \varphi)$, we assume that the electron states are confined to the surface of the free-electron Fermi sphere. The work of Anderson and Gold¹⁵ indicates that the departure of the Fermi surface from a sphere is small, of the order of 10%. In the next section, we discuss the calculation of $F(\omega, \theta, \varphi)$ (and thus in essence the kernel) as a series of angular harmonics.

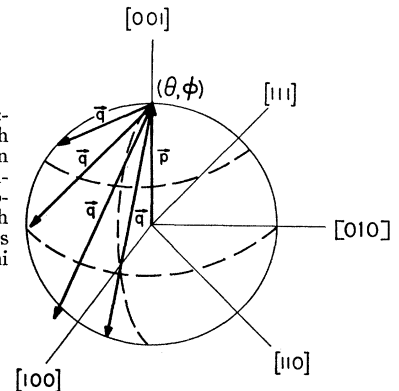


FIG. 2. The free-electron Fermi sphere with some possible phonon wave vectors, \mathbf{q} , connecting the electron momentum state \mathbf{p} with other electron states on or near the Fermi surface.

²⁶ J. M. Rowell, P. W. Anderson, and D. E. Thomas, Phys. Rev. Letters **10**, 334 (1963).

IV. THE DENSITY OF PHONON STATES

The usual dispersion relation between ω and \mathbf{q} is given by considering \mathbf{q} to be defined in the first Brillouin zone. For the purposes of our problem, however, it is more convenient to include umklapp contributions by using a repeated-zone scheme, i.e., by defining a function $\omega(\mathbf{q})$, where \mathbf{q} ranges over all possible values in reciprocal space and

$$\omega(\mathbf{q} + \mathbf{G}_i) = \omega(\mathbf{q}); \quad (4.1)$$

\mathbf{G}_i is any reciprocal lattice vector. As an example, Fig. 3 gives the phonon dispersion curve obtained in this manner from the experiments of Brockhouse *et al.*,¹³ for \mathbf{q} along the $[\bar{1}10]$ direction. The experimental data give the dispersion curves for the three principal symmetry directions $[100]$, $[\bar{1}10]$, and $[111]$. In order to interpolate between these directions, we expanded $\omega(\mathbf{q})$ in the following form:

$$\omega_\lambda(q, \Theta, \Phi) = \sum_n \omega_{n\lambda}(q) K_n(\Theta, \Phi), \quad (4.2)$$

where λ indicates the polarization, q is the magnitude of the wave vector, and Θ, Φ are its polar and azimuthal angles. The K_n are Cubic harmonics,²⁷ suitable linear combinations of spherical harmonics that are invariant under operations of the cubic group. Since the experimental measurements were confined to the three main symmetry directions, we truncate Eq. (4.2) by including only the first three terms. These harmonics are given by

$$K_0 = 1, \\ K_1 = (5.73/r^4)(x^4 + y^4 + z^4 - 0.6r^4) = \frac{5.73}{r^4} [K_1], \quad (4.3)$$

$$K_2 = (147.2/r^6)(x^2y^2z^2 + 0.0455[K_1]r^2 - 0.0095r^6).$$

These three terms include all values up to $l=6$. For each polarization mode, the $\omega_{n\lambda}$ were calculated for 26 values of q equally spaced between 0 and $2p_F$.

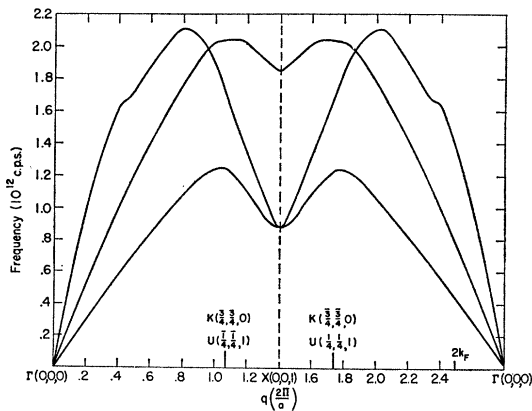


FIG. 3. Dispersion curve for q in the $[\bar{1}10]$ direction, with $\omega(\mathbf{q}) = \omega(\mathbf{q} + \mathbf{G}_i)$.

²⁷ F. C. Von der Lage and H. A. Bethe, Phys. Rev. **71**, 612 (1947).

The calculation of $F(\omega, \theta, \varphi)$ proceeded by considering one state, $\mathbf{p}(\theta, \varphi)$, fixed on the Fermi sphere, and using a random generating function to call other points, $\mathbf{p}'(\theta', \varphi')$, on the sphere. The phonon wave vector, $\mathbf{q} = \mathbf{p} - \mathbf{p}'$, and its associated frequency obtained from Eq. (4.2) were then calculated. The frequency range from 0 to 2.18×10^{12} cps was divided into 88 intervals and the number of occurrences per interval, for a total of 4500 points called, was counted.

In order to be consistent with our approximation for $\omega(\mathbf{q})$, i.e., an expansion in three Cubic harmonics, we also expanded $F^\lambda(\omega, \theta, \varphi)$ in the three lowest harmonics. Since it was assumed that the coupling strengths were the same for all polarizations, in calculating the expan-

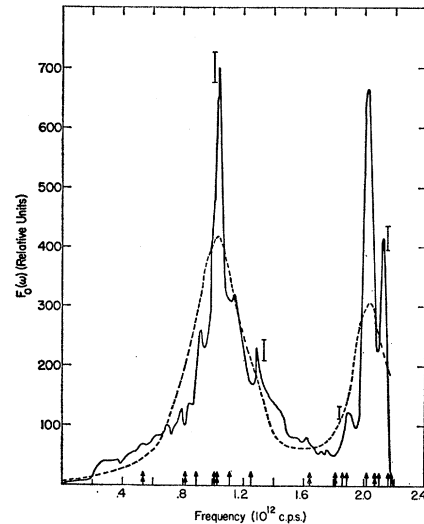


FIG. 4. The isotropic part of the phonon density of states. The solid curve gives the lead phonon density of states $F_0(\omega)$, found by means of the random generating function. Error bars show the uncertainty inherent in that calculation. The dashed line represents the approximate $F_0(\omega)$ used by previous investigators. The single-headed arrows indicate the usual Van Hove singularities expected from a knowledge of the measured ω -versus- q curves. The double-headed arrows indicate additional singularities, which are the result of the particular nature of the density of states that enters the gap equation.

sion coefficients, we first added together, for a given direction, the contributions from all three modes. We obtained then

$$F(\omega, \theta, \varphi) = \sum_\lambda F^\lambda(\omega, \theta, \varphi) \\ = F_0(\omega) + F_1(\omega)K_1(\theta, \varphi) + F_2(\omega)K_2(\theta, \varphi), \quad (4.4)$$

where the coefficients $F_i(\omega)$ were calculated by successively fixing \mathbf{p} in the $[100]$, $[\bar{1}10]$, and $[111]$ directions. Figure 4 shows $F_0(\omega)$; $F_1(\omega)$ and $F_2(\omega)$ are given in Fig. 5.

Before proceeding with the calculation of the energy gap, we digress to discuss the nature of $F_0(\omega)$, the isotropic part of the density of phonon states, and compare it with previous work.

As mentioned in Sec. III, SSW²⁵ approximated $F_0(\omega)$

by a superposition of Lorentzians [Eq. (3.15)]. They used the following parameters:

$$\begin{aligned}\omega_{1l} &= 8.5 \text{ meV}, \\ \omega_{2l} &= 0.5 \text{ meV}, \\ \omega_{1t} &= 4.4 \text{ meV}, \\ \omega_{2t} &= 0.75 \text{ meV},\end{aligned}\quad (4.5)$$

where l and t refer to longitudinal and transverse polarizations, respectively. The density of states with these values of the parameters is plotted in Fig. 4 superimposed on the density of states found in our calculation. The two curves coincide reasonably well, and thus we feel justified in using the previously calculated isotropic gap solutions to calculate the anisotropy.

In addition to the gross features of $F_0(\omega)$, we may consider its detailed structure which, as may be seen from Fig. 4, is very rich. We note that the Kubic interpolation used is such that a minimum number of extra singularities is introduced, since the harmonics are the smoothest type of functions with the required symmetry. This is of experimental interest since McMillan and Rowell²⁸ have shown that tunneling data may be inverted to obtain the density of phonon states. The usual Van Hove singularities in the phonon spectrum have been used^{29,30} to explain various features of the d^2I/dV^2 -versus- V curves obtained. Certain anomalies remain, in particular at low voltages, which are not accounted for by maxima, minima, and saddle points in the phonon $\omega(\mathbf{q})$ curves.

We wish to emphasize some special features²⁸ of the density of phonon states, $F(\omega, \theta, \varphi)$, which enters the gap equation. Although all the usual Van Hove singularities³¹ which appear in the normal density of states also occur in $F(\omega, \theta, \varphi)$, additional ones are present, which must be considered in a complete analysis of the tunneling data.

The normal density of states is defined as

$$F(\omega)d\omega \propto \int_{\omega}^{\omega+d\omega} d^3q. \quad (4.6)$$

However, the density that enters the gap equation is given by

$$F(\omega)d\omega \propto \int_{\omega}^{\omega+d\omega} \mathfrak{N}(\mathbf{q})d^3q, \quad (4.7)$$

where $\mathfrak{N}(\mathbf{q})$ is a function that guarantees that the q vectors connect two points on (or close to) the Fermi surface. For a spherical Fermi surface, $\mathfrak{N}(\mathbf{q})$ is a function only of the magnitude of \mathbf{q} , and independent of

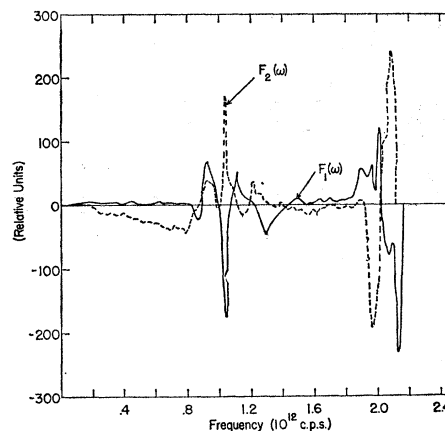


FIG. 5. The anisotropic part of the phonon density of states. The solid curve represents $F_1(\omega)$ and the dashed one— $F_2(\omega)$. The vertical scale is the same as that used in Fig. 4.

angle. In fact

$$\begin{aligned}\mathfrak{N}(q) &= \text{constant} & 0 < q < 2p_F, \\ \mathfrak{N}(q) &= 0 & q > 2p_F.\end{aligned}\quad (4.8)$$

In the case of a general Fermi surface, the function is more complicated. When the \mathbf{q} involved, for example, connects two regions of the surface which are essentially flat and parallel, $\mathfrak{N}(\mathbf{q})$ is large. Thus the forms of the Van Hove-type singularities calculated from Eq. (4.7) may be different than those obtained from Eq. (4.6). Since we assumed a spherical Fermi surface in calculation $F_0(\omega)$, these changes are not of interest in the present comparison.

Additional singularities—ones not present in the usual density of phonon states—should appear because of the singularity in $\mathfrak{N}(q)$, when $q = 2p_F$. We consider first the free-electron case and note that the possible phonon wave vectors fill a sphere of radius $2p_F$. For any given direction, the value of ω associated with $q = 2p_F$ is an extremal value with respect to changes of q in the radial direction. If, in addition, ω is a maximum or minimum with respect to changes of the Cartesian coordinates of the local tangent plane, then ω is a critical value, not present in the usual density. In the case of a general Fermi surface, the same situation may occur when q is a local extremal caliper dimension of the surface and ω is also an extremum with respect to small-changes in the plane perpendicular to \mathbf{q} . For any given direction, more than one extremal dimension may exist, corresponding to both local maxima and minima of q . The usual Van Hove singularities are indicated in Fig. 4. Some of the additional ones, those present in the free-electron model due to q in the three main symmetry directions, are also shown.

V. CALCULATION OF THE ANISOTROPIC GAP

The calculation of the anisotropy was performed using the functions $\Delta_0(p_0)$ and $Z_0(p_0)$ obtained by

²⁸ W. L. McMillan and J. M. Rowell, Phys. Rev. Letters 14, 108 (1965).

²⁹ D. J. Scalapino and P. W. Anderson, Phys. Rev. 133, A921 (1964).

³⁰ J. M. Rowell and L. Kopf, Phys. Rev. 137, A907 (1965).

³¹ L. Van Hove, Phys. Rev. 89, 1189 (1953).

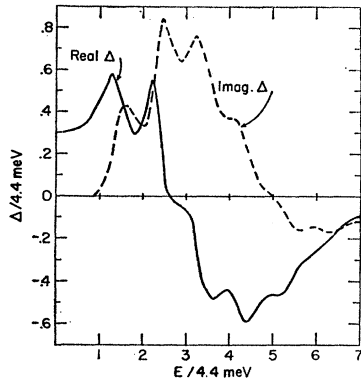


FIG. 6. The real and imaginary parts of Δ as calculated by Swihart for isotropic lead.

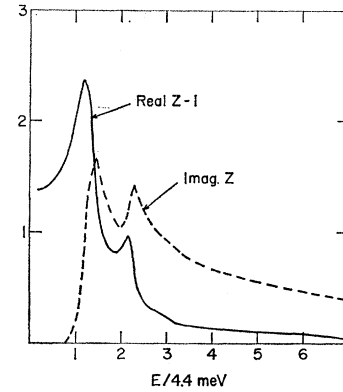


FIG. 7. The real and imaginary parts of Z as calculated by Swihart for isotropic lead.

Swihart,³² which are essentially the same as those found by SSW.²⁵ He used a lower cutoff of $\omega_{cf} = 0.774\omega_{1t}$, i.e.,

$$F(\omega) = 0 \quad \omega < \omega_{cf} \quad (5.1)$$

which we, for consistency, also employ. Swihart's curves for the real and imaginary parts of Δ_0 and Z_0 are given in Figs. 6 and 7. The value of the coupling parameter was determined by demanding that the isotropic density of states, $F_0(\omega)$, reproduce Swihart's values of the isotropic gap for $p_0 = \Delta_{\text{BCS}}$. The fact that by using that value of the coupling constant we were able to reproduce, within approximately 3%, the isotropic gap for values of p_0 in the range $\Delta_{\text{BCS}} < p_0 < 2\Delta_{\text{BCS}}$ is another indication that the calculated $F_0(\omega)$ and the density of states used by Swihart and SSW are compatible.

$$R_j^1(p_0) = N(0) \int_{\Delta_{\text{BCS}}}^{\omega_c} d p_0' \operatorname{Re} \left[\frac{\Delta_0(p_0')}{(p_0'^2 - \Delta_0^2(p_0'))^{1/2}} \right] \left[\int_{\omega_{cf}}^{\omega_{\text{max}}} F_j(\omega) \left(\frac{1}{p_0' + p_0 + \omega - i\delta} + \frac{1}{p_0' - p_0 + \omega - i\delta} \right) d\omega - U_c \delta_{1j} \right], \quad (5.8)$$

$$R_j^2 = N(0) \int_{\Delta_{\text{BCS}}}^{\omega_c} d p_0' \operatorname{Re} \left[\frac{p_0'}{(p_0'^2 - \Delta_0^2(p_0'))^{1/2}} \right] \left[\int_{\omega_{cf}}^{\omega_{\text{max}}} F_j(\omega) \left(\frac{1}{p_0' + p_0 + \omega - i\delta} - \frac{1}{p_0' - p_0 + \omega - i\delta} \right) d\omega \right], \quad (5.9)$$

ω_{max} is the highest phonon frequency $\cong 2.17 \times 10^{12}$ cps, and $N(0)U_c = 0.14$.

As will be discussed below, our primary interest is in $\Delta(p_0)$ for values of p_0 near Δ_{BCS} , the threshold. Table I gives values of the isotropic and anisotropic parts of R^1 and Z for several values of p_0 . Table II gives the values of the energy gap, for a spherical Fermi surface, in the

TABLE I. The various quantities, for three values of p_0 , that enter Eq. (5.7), the expression for the energy gap.

p_0 (meV)	R_0^1 (meV)	R_1^1 (meV)	R_2^1 (meV)	Z_0	Z_1	Z_2
1.38	3.22	0.0477	0.185	2.398	-0.0165	+0.0731
1.71	3.30	0.0497	0.190	2.417	-0.0166	+0.0741
2.61	3.65	0.0515	0.206	2.499	-0.0171	+0.0792

³² J. C. Swihart (private communication).

We now describe the actual calculation of the gap anisotropy. We use the following expansions:

$$R^1(p_0, \theta, \varphi) = Z(p_0, \theta, \varphi) \Delta(p_0, \theta, \varphi) = R_0^1(p_0) + R_1^1(p_0) K_1(\theta, \varphi) + R_2^1(p_0) K_2(\theta, \varphi), \quad (5.2)$$

$$R^2(p_0, \theta, \varphi) = [1 - Z(p_0, \theta, \varphi)] p_0 = R_0^2(p_0) + R_1^2(p_0) K_1(\theta, \varphi) + R_2^2(p_0) K_2(\theta, \varphi), \quad (5.3)$$

where

$$Z_0(p_0) = 1 - R_0^2(p_0)/p_0, \quad (5.4)$$

$$Z_1(p_0) = -R_1^2(p_0)/p_0, \quad (5.5)$$

$$Z_2(p_0) = -R_2^2(p_0)/p_0, \quad (5.6)$$

and

$$\Delta(p_0, \theta, \varphi) = R^1(p_0, \theta, \varphi) / Z(p_0, \theta, \varphi). \quad (5.7)$$

The integrals evaluated were:

three principal symmetry directions. Figure 8 shows the gap in the (110) plane through Γ .

VI. BAND STRUCTURE EFFECTS. ACCURACY OF THE CALCULATION

The results of a variety of experiments—magneto-resistance,³³ ultrasonic attenuation,³⁴ cyclotron reso-

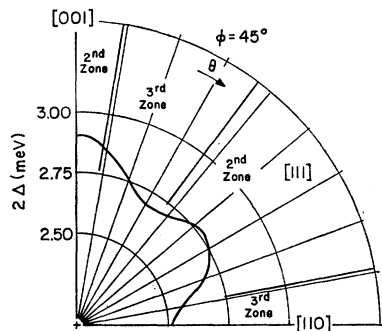
TABLE II. The energy gap, at the threshold, with and without the inclusion of band structure effects.

Crystallographic direction	[100]	[110]	[111]
Energy gap with no account taken of the effects of band structure (meV)	1.46	1.25	1.38
Energy gap with the effects of band structure included (meV)	1.43	1.28	1.38

³³ E.g., J. E. Schirber, Phys. Rev. **131**, 2459 (1963).

³⁴ E.g., J. A. Rayne, Phys. Rev. **129**, 652 (1963).

FIG. 8. The double gap in the (110) plane through Γ , with no account taken of the effects of crystal potential mixing.

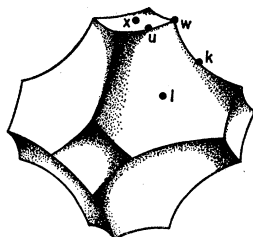


nance³⁵—attest to the fact that the Fermi surface of lead is described quite well by the nearly-free-electron model. Recently Gold and Anderson,¹⁵ using the de Haas-van Alphen effect, have measured a large number of the extremal cross-sectional areas of the lead Fermi surface. They were able to describe the surface, using a four-plane wave interpolation scheme with two pseudo-potential matrix elements, a spin-orbit coupling factor, and the Fermi energy as adjustable parameters. The values of these parameters were determined by means of a least-squares fit to eight of the observed areas. It was found that the spin-orbit coupling factor was necessary to obtain any reasonable fit to all the areas.

The free-electron Fermi surface has pieces in the second, third, and fourth Brillouin zones. Experiment, however, shows that the energy gaps at the relevant points are large enough to remove all electrons from the fourth zone. This is also a feature of the Gold and Anderson model. Figure 9 shows the second zone free electron hole surface (reduced zone scheme); Fig. 10 represents the third zone electron surface (repeated zone scheme). From Fig. 11, a cross section in the (110) plane through Γ , we see that the deviation of the four-parameter model from the free-electron sphere is large only in the region of the Brillouin-zone boundaries.

In order to consider the effect of the crystal potential, we may assume that the actual wave functions can be expressed as linear combinations of a few functions of a plane-wave character, orthogonalized plane waves (OPW), for example. The effect of the mixing on the anisotropy is taken into account by a procedure essen-

FIG. 9. The second Brillouin zone hole surface of lead, according to the free-electron model (from Ref. 15).



³⁵ E.g., R. Mina and M. S. Khaikin, Zh. Eksperim. i Teor. Fiz. 45, 1304 (1963) [English transl.: Soviet Phys.—JETP 18, 896 (1964)].

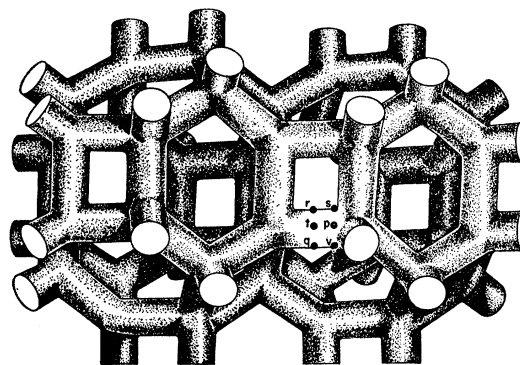


FIG. 10. A schematic representation of the third Brillouin zone electron surface of lead in the repeated-zone scheme (from Ref. 15).

tially the same as that used by Anderson³⁶ in his theory of dirty superconductors.

An actual electronic state $|n\rangle$ is considered to be of the form

$$|n\rangle = \sum_{p,\sigma} A_{np\sigma} |p/\sigma\rangle, \quad (6.1)$$

where $|p/\sigma\rangle$ indicates an OPW of wave vector p and spin σ .

When no magnetic field is present, the time-reversed state $| -n\rangle$ is an eigenfunction of the Hamiltonian with the same energy. In general, Cooper pairing consists of coupling of the states $|n\rangle$ and $| -n\rangle$. The gap equation is then given by

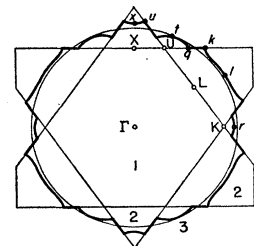
$$\Delta_n = \sum_{n'} \frac{V_{nn'} \Delta_{n'}}{2E_{n'}}. \quad (6.2)$$

If, for example,¹⁹ the Bardeen-Pines interaction¹⁷ is considered,

$$-V_{nn'} = \sum_{p,p',\sigma,\sigma'} \frac{|A_{np\sigma}|^2 |A_{n'p'\sigma'}|^2 |g_{p'p}|^2 \hbar\omega_{p-p'}}{(\epsilon_n - \epsilon_{n'})^2 - \hbar^2\omega_{p-p'}^2}. \quad (6.3)$$

In the case of crystal potential mixing, in contrast to the impurity scattering originally considered by Anderson, the energies of all the plane waves $|p\rangle$ which mix strongly in a given state $|n\rangle$ are almost the same. Hence, in the denominator of Eq. (6.3), we may assume that

FIG. 11. (110) Cross section through Γ of the lead Fermi surface in the extended zone scheme. The heavy curve (the four-parameter surface) is compared with the free-electron circle (from Ref. 15).



³⁶ P. W. Anderson, J. Phys. Chem. Solids 11, 26 (1959).

$\epsilon_n = \epsilon_{\mathbf{p}}$, $\epsilon_{n'} = \epsilon_{\mathbf{p}'}$. With this assumption, the quantity $V_{nn'}$ is given by a weighted average

$$V_{nn'} = \sum_{\mathbf{p}, \mathbf{p}', \sigma, \sigma'} |A_{n\mathbf{p}\sigma}|^2 |A_{n'\mathbf{p}'\sigma'}|^2 V_{\mathbf{p}\mathbf{p}'}, \quad (6.4)$$

where $V_{\mathbf{p}\mathbf{p}'}$ is the interaction in the absence of mixing.

We now distinguish two regions of interest—the first occupies 90% of the area of the Fermi surface and

comprises the part not near a Brillouin-zone boundary, where the one OPW approximation is good; the second region includes the remaining portions of the Fermi surface, where the mixing is strong. In the first region,

$$A_{n\mathbf{p}\sigma} = \delta_{\mathbf{p}\mathbf{p}_1} \delta_{\sigma\sigma_1}, \quad (6.5)$$

and thus for $|n\rangle$ in that region, we have

$$\Delta_{\mathbf{p}_1} = \sum_{n', \mathbf{p}', \sigma'} \frac{|A_{n'\mathbf{p}'\sigma'}|^2 \Delta_{n'} V_{\mathbf{p}_1\mathbf{p}'}}{2E_{n'}} = \sum_{\text{REGION 1}} \frac{\Delta_{\mathbf{p}_1'} V_{\mathbf{p}_1\mathbf{p}_1'}}{2E_{\mathbf{p}_1'}} + \sum_{\text{REGION 2}} \frac{|A_{n'\mathbf{p}'\sigma'}|^2 \Delta_{n'} V_{\mathbf{p}_1\mathbf{p}'}}{2E_{n'}}. \quad (6.6)$$

The second sum on the right-hand side of the equation is over only approximately 10% of the Fermi surface, and the error made by assuming that even in that region

$$A_{n'\mathbf{p}'\sigma'} = \delta_{\mathbf{p}'\mathbf{p}_2} \delta_{\sigma'\sigma_2'}, \quad (6.7)$$

is small. The anisotropic part of the gap is, as calculated above, approximately 10%, and the second sum contributes approximately only 10% of the value of $\Delta_{\mathbf{p}_1}$. Hence, the error is of the order of 1% of $\Delta_{\mathbf{p}_1}$, and the energy gap is essentially unchanged by the crystal potential for values of \mathbf{p} away from the Brillouin-zone walls.

When $|n\rangle$ is in the second region, we have

$$\Delta_n = \sum_{\mathbf{p}, \sigma, n', \mathbf{p}', \sigma'} \frac{|A_{n\mathbf{p}\sigma}|^2 |A_{n'\mathbf{p}'\sigma'}|^2 \Delta_{n'} V_{\mathbf{p}\mathbf{p}'}}{2E_{n'}} = \sum_{\mathbf{p}\sigma} |A_{n\mathbf{p}\sigma}|^2 \left[\sum_{\text{REGION 1}} \frac{\Delta_{\mathbf{p}_1'} V_{\mathbf{p}\mathbf{p}_1'}}{2E_{\mathbf{p}_1'}} + \sum_{\text{REGION 2}} \frac{|A_{n'\mathbf{p}'\sigma'}|^2 \Delta_{n'} V_{\mathbf{p}\mathbf{p}'}}{2E_{n'}} \right]. \quad (6.8)$$

Again, the error introduced by letting Eq. (6.7) hold in the second term is of the order of 1%, and we find that for n in region 2

$$\Delta_n = \sum_{\mathbf{p}\sigma} |A_{n\mathbf{p}\sigma}|^2 \Delta_{\mathbf{p}}. \quad (6.9)$$

In order to calculate the mixing coefficients $A_{n\mathbf{p}\sigma}$ we have used the four OPW approximation of Anderson and Gold, with the values of the parameters which they determined. The energy gap, in the (110) plane through Γ , obtained from Eq. (6.9) is shown in Fig. 12. The values of the gap for the three principal symmetry directions are given in Table II. As expected, the mixing tends to reduce the anisotropy. It must be emphasized, however, that the correction is only significant in a small part of the Fermi surface. Figure 13 is a schematic

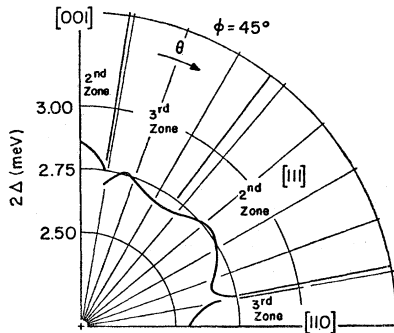


FIG. 12. The double-energy gap (meV) in the (110) plane through Γ , after the effects of band structure have been included.

representation of the energy gap on the electron and hole surfaces. Table III lists the various critical points (maxima, minima and saddle points) of the gap function.

In order to obtain some very rough idea as to the accuracy of our calculation of the gap anisotropy due to the band structure and phonon density of states, we note the following sources of error:

- experimental errors in Brockhouse's phonon data,
- approximation of $\omega(\mathbf{q})$ by three Kubic harmonics,
- "random" calculation of $F(\omega, \theta, \varphi)$,
- approximation of $F(\omega, \theta, \varphi)$ by three Kubic harmonics,
- errors in numerical procedures,
- failure to iterate the first-order solution of the gap anisotropy.

Brockhouse's phonon dispersion data were taken with an accuracy of approximately 3%. Using the effects of translational symmetry, we estimate that the error due to the truncated expansion of $\omega(\mathbf{q})$ is of the order of 15% of its anisotropy. These two sources of error, coupled to the inherent $N^{1/2}$ -type error of the random generating function calculation, lead to an error of the order of 20% on the $F(\omega, \theta, \varphi)$ calculated for the three (θ, φ) directions in Sec. IV. This error coupled to the error of the order of 10% of the density of states anisotropy introduced by the truncated expansion of $F(\omega, \theta, \varphi)$ leads to an error of perhaps 30% in the coefficients $F_i(\omega)$. The calculations were performed on the IBM 7094 complex

of the University of Chicago computation center. The calculational errors are negligible compared with the other errors discussed here. Since the various R_i^1 and Z_i coefficients are directly proportional to an integral of the F_i , they are calculated with an uncertainty of about 35% as a result of the errors from the first four sources in the above list. The last source of error, i.e., our failure to iterate the first solution obtained for the anisotropic gap, is more difficult to estimate. In essence, however, the solution is good to first order in the anisotropy, and further iteration would introduce corrections of the order of 10%. Considering all major sources of error and assuming that some cancellation of the various errors occur, we estimate that the uncertainty in our calculation of the anisotropic part of the energy gap, i.e., that anisotropic part due to the band structure plus phonon density of states, is less than 30% of its value.

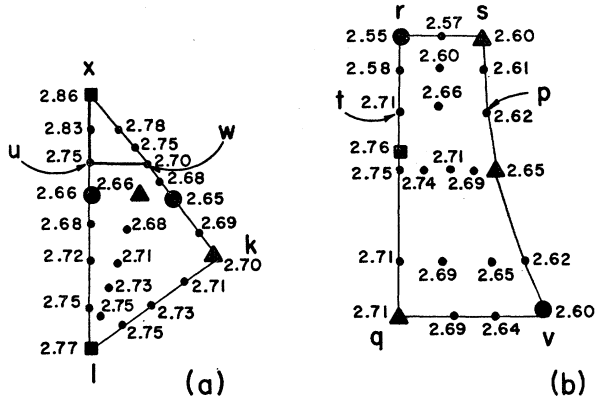


FIG. 13. The double-energy gap (meV) on (a) the second-zone hole surface, (b) the third-zone electron surface. The small Roman letters refer to the corresponding points in Figs. 9 and 10. The squares, triangles, and circles indicate maxima, saddle points, and minima, respectively.

VII. COMPARISON WITH EXPERIMENT

When considering experiments that display the anisotropy of the energy gap, we must distinguish three different regimes. The first, and least interesting from the standpoint of anisotropy, is the dirty limit. Here either surface effects are so strong and/or the impurity content so high that rapid scattering takes place between Bloch-like states, i.e., the mean free path is very short and a mixing mechanism, as discussed by Anderson,³⁶ smoothes out all anisotropy. This is the region in which only an isotropic $\Delta_0(p_0)$ exists.

The second regime is that in which the mean free path is finite, but long enough for anisotropic effects to remain. A polycrystalline sample is such a system. The anisotropic energy gap is still well defined for each crystallite, but the experiments measure only averages. We expect that, for directional experiments, all crystallographic directions contribute equally.

The third regime—the one which most clearly reveals

TABLE III. The maxima, minima, and saddle points of the double energy gap on the second- and third-zone pieces of the Fermi surface.

Critical point	Second-zone hole surface		Third-zone electron surface		
	Minima (meV)	2.66	2.65	2.60	2.55
Saddle points (meV)	2.70	2.66	2.71	2.65	2.60
Maxima (meV)	2.86	2.77		2.76	

anisotropy—is that of the pure single crystal. Here the mean free path is very long, minimal mixing occurs, and for directional experiments, only some crystallographic directions contribute appreciably.

Unfortunately, from the experimental point of view, the technical problems involved in the preparation of single crystal lead films for tunneling or other relevant experiments are severe. Hence, one cannot neglect the second regime as a source of information.

We will investigate the effects of anisotropy by means of what is essentially a singularity analysis, i.e., a search for singularities in experimental observables due to extrema and other critical values of the gap. The analysis is confined to effects which are associated with low-energy quasiparticles, i.e., excitation energies of the order of the energy gap. These include the so-called threshold phenomena. A consideration of the isotropic gap function pictured in Fig. 6 and the values given in Table I shows that, for these effects, the function Δ may be considered to be independent of energy. In addition, the imaginary part of Δ is equal to zero in this region. This enables us to concentrate on the effects of anisotropy, and not concern ourselves with effects connected with the strong-coupling nature of the superconductivity in lead.

Whenever possible, we treat the zero-temperature case. In general, a higher temperature will tend to smooth singularities, but their basic nature will remain the same.

A. Tunneling Experiments

The most direct method of observing anisotropy is by means of tunneling experiments through an insulating layer between two superconductors, or between a superconductor and a normal metal.³⁷ The Hamiltonian³⁸⁻⁴⁰ giving rise to tunneling can be assumed to be of the form

$$H = H_R + H_L + H_T, \quad (7.1)$$

where H_R and H_L are the Hamiltonians for electrons in the right and left metals, respectively, and H_T is a coupling (tunneling) term proportional to a matrix element $T_{pp'}$,⁴¹ which will be discussed below. Second-

³⁷ E.g., I. Giaever and K. Megerle, Phys. Rev. **122**, 1101 (1961).

³⁸ J. Bardeen, Phys. Rev. Letters **6**, 57 (1961).

³⁹ M. H. Cohen, L. M. Falicov, and J. C. Phillips, Phys. Rev. Letters **8**, 316 (1962).

⁴⁰ R. E. Prange, Phys. Rev. **131**, 1083 (1963).

⁴¹ W. A. Harrison, Phys. Rev. **123**, 85 (1961).

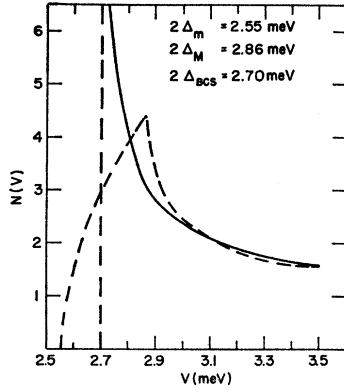


FIG. 14. The tunneling density of states, when the distribution of gap values is a constant between the minimum gap, Δ_m , and the maximum gap, Δ_M , and is zero elsewhere. A BCS density of states with $\Delta_{BCS} = \frac{1}{2}(\Delta_m + \Delta_M)$ is also shown.

order perturbation theory, i.e., the use of Fermi's golden rule, yields the tunneling current

$$I(eV) = \frac{2\pi e}{\hbar} \sum_{\mathbf{p}, \mathbf{p}'} |T_{\mathbf{p}\mathbf{p}'}|^2 \times [f(\epsilon_{\mathbf{p}}) - f(\epsilon_{\mathbf{p}'} + eV)] \delta(\epsilon_{\mathbf{p}} - \epsilon_{\mathbf{p}'}), \quad (7.2)$$

where V is the voltage applied between the two materials and f is the Fermi function. There are, as mentioned above, two experimental regimes of interest, the single crystal and polycrystal. We first consider only polycrystalline materials. The various crystallites are oriented in different ways with respect to the normal of the tunneling surface. For such materials, the angular summation in Eq. (7.2) is an effective average over $T_{\mathbf{p}\mathbf{p}'}$. The assumption that $|T_{\mathbf{p}\mathbf{p}'}|^2$ is independent of energy⁴² enables us then to replace it by an average matrix element T , and to rewrite Eq. (7.2) as

$$I(eV) = P \int_{-\infty}^{\infty} dE N_T^R(E) \times N_T^I(E + eV) [f(E) - f(E + eV)], \quad (7.3)$$

where $P = (2\pi e/\hbar) |T|^2$ and the $N_T(E)$ are effective densities of states, given by

$$N_T(E) = -\frac{N(0)}{4\pi^2} \int_{-\infty}^{\infty} d\epsilon_{\mathbf{p}} \int_{-1}^1 d(\cos\theta) \times \int_0^{2\pi} d\varphi \text{Im} \mathbf{G}(\mathbf{p}, E) \quad (7.4)$$

TABLE IV. The form of the gap distribution function $f(x)$ in the vicinity of critical values Δ_c of $\Delta(\theta, \varphi)$.

Critical point	$x < \Delta_c$	$x > \Delta_c$
Minimum	C	$C + D$
Saddle point	$C' - D' \lg[1 - (x/\Delta_{SP})]$	$C' - D' \lg[(x/\Delta_{SP}) - 1]$
Maximum	$C'' + D''$	C''

⁴² In considering $T_{\mathbf{p}\mathbf{p}'}$, we have also ignored the variation of the magnitude of the velocity with position on the Fermi surface. This has no essential effect on the results of the singularity analysis employed.

for a superconductor, and

$$N_T(E) = N(0) \quad (7.5)$$

for a normal metal. Here $\mathbf{G}(\mathbf{p}, E)$ is the Green's function introduced in Sec. III. Integration of Eq. (7.4) over $\epsilon_{\mathbf{p}}$ gives

$$N_T(E) = \frac{N(0)}{4\pi^2} \int_{-1}^1 d(\cos\theta) \int_0^{2\pi} d\varphi \times \text{Re} \left[\frac{E}{(E^2 - \Delta^2(E, \theta, \varphi))^{1/2}} \right]. \quad (7.6)$$

We shall be concerned with tunneling near the threshold, and hence $\Delta(E, \theta, \varphi)$ may be considered real and independent of E . It is useful to transform Eq. (7.6) in the following fashion

$$N_T(E) = \frac{N(0)}{4\pi^2} \int_{x_{\min}}^E \frac{E}{(E^2 - x^2)^{1/2}} f(x) dx, \quad (7.7)$$

where

$$f(x) = \frac{1}{4\pi^2} \int_{-1}^1 d(\cos\theta) \int_0^{2\pi} d\varphi \delta[x - \Delta(\theta, \varphi)]. \quad (7.8)$$

When $\Delta(\theta, \varphi)$ is independent of angle,

$$f(x) = \delta(x - \Delta), \quad (7.9)$$

and

$$N_T(E) = N(0) \text{Re}[E/(E^2 - \Delta^2)^{1/2}], \quad (7.10)$$

the expression used by SSW.

As an example of the changes that gap anisotropy may introduce, we first consider the effect of having

$$f(x) = F \quad (7.11)$$

for values of Δ between Δ_m and Δ_M , the minimum and maximum values of the gap. Performing the integration

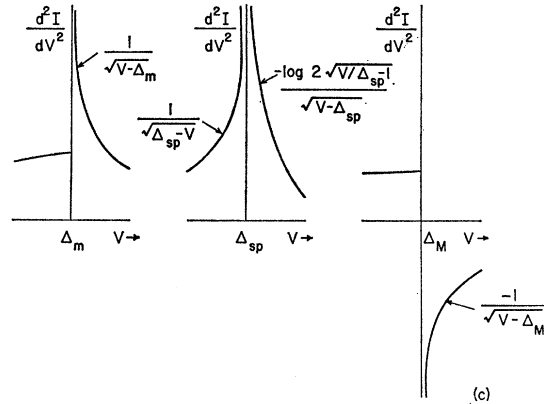


FIG. 15. The form of d^2I/dV^2 for a superconductor-normal metal junction, when V is in the vicinity of a critical value Δ_c . (a) $\Delta_c = \Delta_m$ (a minimum), (b) $\Delta_c = \Delta_{SP}$ (a saddle point), (c) $\Delta_c = \Delta_M$ (a maximum). Here $eV \equiv V$.

TABLE V. The leading terms of dI/dV and d^2I/dV^2 for a superconductor-normal metal junction, when eV is in the vicinity of a critical value Δ_c of $\Delta(\theta, \varphi)$. The A and B are constants which depend on details of $f(x)$, the gap distribution function.

Critical point	dI/dV		d^2I/dV^2	
	$eV \leq \Delta_c$	$eV \geq \Delta_c$	$eV \leq \Delta_c$	$eV \geq \Delta_c$
Minimum	continuous	A	$(A+B) + (\sqrt{2}/\pi)B\Delta_m^{1/2}(eV - \Delta_m)^{-1/2}$	
Saddle point	continuous	$A' + B'(\Delta_{SP} - eV)^{-1/2}$	$A' - \frac{(2/\pi)B'g_2[(eV - \Delta_{SP})/\Delta_{SP}]^{1/2}}{(eV - \Delta_{SP})^{1/2}}$	
Maximum	continuous	$A'' + B''$	$A'' - (\sqrt{2}/\pi)B''\Delta_M^{1/2}(eV - \Delta_M)^{-1/2}$	

in Eq. (7.7), we find

$$\frac{N_T(E)}{N(0)} = FE \left(\sin^{-1} \frac{\Delta_M}{E} - \sin^{-1} \frac{\Delta_m}{E} \right), \quad (7.12)$$

for $E > \Delta_M$, and

$$N_T(E)/N(0) = FE \left(\frac{1}{2}\pi - \sin^{-1}(\Delta_m/E) \right) \quad (7.13)$$

for $\Delta_m < E < \Delta_M$. Figure 14 shows this form of $N_T(E)$ together with a curve of the BCS form

$$N_T(E)/N(0) = E/(E^2 - \Delta_{\text{BCS}}^2)^{1/2}, \quad (7.14)$$

where $\Delta_{\text{BCS}} = \frac{1}{2}(\Delta_m + \Delta_M)$. The two curves are normalized so that they approach the same limit as $E \rightarrow \infty$. We can see that the general effect of anisotropy is to broaden the density of states.

In order to consider the effects of the critical points of $\Delta(\theta, \varphi)$ on $N_T(E)$, we first notice that the two-dimensional Van Hove³¹ theorems apply to $f(x)$. This may be understood by noting that, in the vicinity of a point (θ, φ) on the unit sphere, the difference in area defined by the Cartesian coordinates in the tangent plane at the point and the corresponding area on the sphere is given by $[1 - \cos \zeta]$, where ζ is the angle between a given direction and the point of contact. This is a second-order effect which does not, to lowest order, change the values of the integrals evaluated by Van Hove to obtain the form of his singularities. Table IV gives the form of the distribution function (7.8) about a maximum, minimum, and saddle point of $\Delta(\theta, \varphi)$.

For a superconductor-normal metal junction at

$$T=0,$$

$$dI/dV = PeN_T(eV), \quad (7.15)$$

$$\frac{d^2I}{dV^2} = \frac{PedN_T(E)}{dE} \Big|_{E=eV}. \quad (7.16)$$

The use of Eq. (7.7) and the expansion forms of $f(x)$ about Δ_c , a critical value of $\Delta(\theta, \varphi)$, yields the form of $N(E)$ when E is close to Δ_c . In the Appendix, we give, as an example, the calculation for a local minimum value of the energy gap. The analytic forms of dI/dV and d^2I/dV^2 corresponding to various types of critical points in $\Delta(\theta, \varphi)$ are given in Table V. Figure 15 shows the results for d^2I/dV^2 graphically. The various singularities obtained tend to be smeared out at finite temperatures. A similar analysis may be performed for a superconductor-superconductor junction. As is well known,⁴³ in the case of isotropic materials, a jump discontinuity is present in the I versus V curves for $eV = \Delta_1 + \Delta_2$, even for temperatures greater than zero. We considered the case in which one of the superconductors is isotropic, i.e., its gap is a constant Δ_1 independent of angle, and the second superconductor has an anisotropic gap $\Delta_2(\theta, \varphi)$. We have calculated the form of dI/dV and d^2I/dV^2 at zero temperature for eV in the vicinity of $\Delta_1 + \Delta_{2c}$, where Δ_{2c} is a critical value of $\Delta_2(\theta, \varphi)$. In the Appendix, we show the calculation for the jump in dI/dV at $eV = \Delta_1 + \Delta_{2c}$, when Δ_{2c} is a minimum. The analytic forms of dI/dV and d^2I/dV^2 are given in Table VI. The results are presented graphically in Fig. 16. As expected, the singularities are

TABLE VI. The leading terms of dI/dV and d^2I/dV^2 for an isotropic superconductor, (1) anisotropic superconductor, (2) junction, when eV is in the vicinity of $\Delta_1 + \Delta_{2c}$, where Δ_{2c} is a critical value of $\Delta_2(\theta, \varphi)$. The F , G , and H are constants which depend on details of $f(x)$, the gap distribution function.

Critical point	dI/dV		d^2I/dV^2	
	$eV \leq \Delta_c$	$eV \geq \Delta_c$	$eV \leq \Delta_c$	$eV \geq \Delta_c$
Minimum	$-F$	$-F + G(\Delta_1\Delta_m)^{1/2}$	$+G(\Delta_1\Delta_m)^{1/2}e\delta(eV - \Delta_m - \Delta_1)$	
Saddle point	$-F' + G'(eV - \Delta_{SP} - \Delta_1)$	$H'g(eV - \Delta_{SP} - \Delta_1)$	$eG' \frac{eH'(eV - \Delta_{SP} - \Delta_1)^{-1}}{eV - \Delta_{SP} - \Delta_1}$	
Maximum	$-F''$	$-F'' - G''(\Delta_1\Delta_M)^{1/2}$	$-G''(\Delta_1\Delta_M)^{1/2}e\delta(eV - \Delta_M - \Delta_1)$	

⁴³ E.g., D. H. Douglass, Jr., and L. M. Falicov in *Progress in Low Temperature Physics*, edited by C. J. Gorter (North-Holland Publishing Company, Amsterdam, 1964), p. 97.

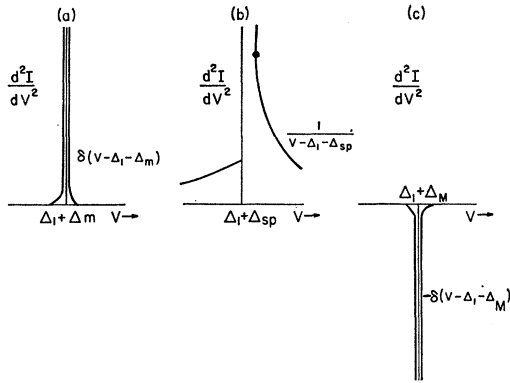


FIG. 16. The form of d^2I/dV^2 for an isotropic superconductor, (1) and polycrystalline anisotropic superconductor, (2) junction when V is in the vicinity of $\Delta_1 + \Delta_{2c}$. (a) $\Delta_{2c} = \Delta_m$ (a minimum), (b) $\Delta_{2c} = \Delta_{sp}$ (a saddle point), (c) $\Delta_{2c} = \Delta_M$ (a maximum). Here $eV \equiv V$.

stronger than those in the corresponding curves of the superconductor-normal metal junction. The jump discontinuity in dI/dV , for Δ_{2c} corresponding to a minimum, may be compared with the similar singularity in the current when both superconductors are isotropic. Figure 17(a) shows the various singularities that will be seen with polycrystalline lead samples. In our approximation, four minima, five saddle points, and three maxima occur.

We now focus our attention on the singularities expected when the superconductors are single crystals,

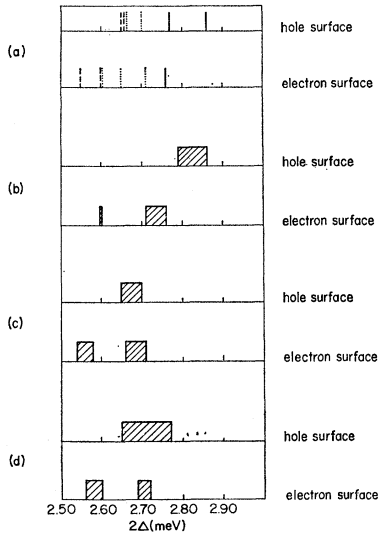


FIG. 17. (a) The energies for which singularities are expected in the tunneling curves of a polycrystalline anisotropic superconductor. The contributions of the electron and hole surfaces are presented separately. Solids lines indicate maxima, dashed lines indicate minima, and dotted lines indicate saddle points. (b), (c), (d) The range of gap values included within the areas on the Fermi surface of a single crystal anisotropic superconductor that contribute for tunneling in the $[100]$, $[110]$, and $[111]$ directions, respectively. The contributions of the electron and hole surfaces are, in each case, presented separately.

rather than polycrystals. We begin again with Eq. (7.2) and consider the tunneling matrix element $T_{pp'}$ in order to determine which carriers will contribute most for the normal to the barrier oriented in a particular crystal direction. Using the independent particle model and the WKB approximation, Harrison⁴¹ has derived an expression for $T_{pp'}$

$$|T_{pp'}|^2 \propto \delta_{p_{11}, p_{11}'} \exp \left[-2 \int_{x_l}^{x_r} \phi_1(x) dx \right], \quad (7.17)$$

where ϕ_{11} and ϕ_1 are the components of the electron momentum parallel and perpendicular to the barrier, and x_r , x_l are the classical turning points in the right and left metals.

For parabolic energy bands with a free-electron mass, we use the approximate expression

$$|T_{pp'}|^2 \propto \delta_{p_{11}, p_{11}'} \times \exp \left[-\eta \int_{x_l}^{x_r} (U(x) + E_F - E_F \cos^2 \gamma)^{1/2} dx \right], \quad (7.18)$$

where $U(x) + E_F$ is the height of the effective barrier, γ is the angle between the electron momentum and the barrier normal, and

$$\eta = 2(2m)^{1/2}/\hbar = 1.025 \text{ eV}^{-1/2} \text{ \AA}^{-1}.$$

In order to obtain an expression for γ_{HM} , the angle for which the matrix element squared is equal to one half its value for $\gamma=0$, we take $U(x) = U_{AV}$ and obtain

$$\cos^2 \gamma_{HM} = 1 - \frac{2(\ln 2) U_{AV}^{1/2}}{1.025(x_r - x_l) E_F} \frac{(\ln 2)^2}{(1.025)^2 (x_r - x_l)^2 E_F}. \quad (7.19)$$

Using the typical values $d = 20 \text{ \AA}$, $E_F = 9.5 \text{ eV}$, and $U_{AV} = 1 \text{ eV}$, we find $\gamma_{HM} \cong 5^\circ$.

Thus, for a spherical Fermi surface, the electrons that contribute strongly are those whose quasiparticle momenta are within approximately 5° of the tunneling direction. For a general band structure, this same condition holds except that the electron velocity rather than the electron momentum should be considered. We now assume that the exponential-like behavior of Eq. (7.18) may be approximated by a cutoff at 5° , i.e., electrons whose velocities are within 5° of the tunneling direction contribute with equal weight and all other electrons make no contribution. Figure 18(a) is a schematic picture of the hole surface which shows the areas that contribute for $\langle 001 \rangle$, $\langle 110 \rangle$, $\langle 111 \rangle$ tunneling directions. Figure 18(b) is a similar sketch of the electron surface. Figures 17(b), 17(c), and 17(d) give the values of the energy gap included within the areas associated with tunneling in each of the principal symmetry directions. If the range of gap values from a given area includes a critical value, i.e., a local maximum,

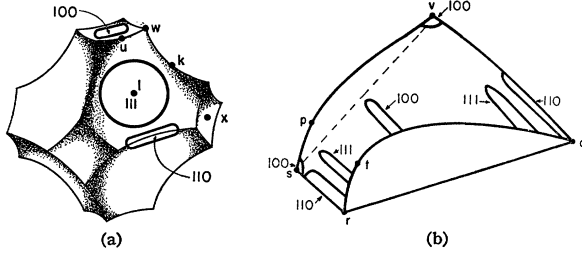


FIG. 18. (a) The second-zone hole surface with the areas shown that contribute for tunneling in the three main symmetry directions. (b) A section of the third-zone electron surface with the areas shown that contribute for tunneling in the three main symmetry directions.

local minimum, or saddle point, then we expect to observe the singularity in the tunneling spectrum associated with that critical value. Such cases may be recognized by comparing Figs. 17(b), 17(c), and 17(d) with Fig. 17(a), and then using Fig. 13 to ascertain the source, i.e., the area of origin, of the singularities of the latter figure. In addition, the minimum and maximum value of the gap within a given area tend to broaden the tunneling characteristics and effective density of states, as was discussed above for the case of Eq. (7.11). If the range of energy values from a given area is very narrow, because the velocity direction changes very rapidly and/or $\Delta(\theta, \varphi)$ varies slowly in the region, we then expect the structure typical of isotropic superconductors to be present in the tunneling curves.

B. Electromagnetic Absorption

In considering the absorption of electromagnetic radiation by superconducting lead, we choose to ignore the precursor absorption,⁴⁴ i.e., the structure appearing just before the main edge. This structure is probably due to a collective mode, and is not directly connected with anisotropy of the energy gap.⁴⁵ The latter is shown by the persistence of the anomaly in heavily doped lead, i.e., lead with a high content of impurities, where the gap is isotropic. If, in addition, the coherence length ξ is assumed to be greater than the penetration depth δ , one may obtain the essential behavior of lead in an electromagnetic field by ignoring all but first order effects.

The current is given by

$$J_i(q) = (i/\omega) P_{ij}(q) E_j(q), \quad (7.20)$$

where $(i/\omega) P_{ij}$ is the conductivity tensor, and E_j is the electric field. In general, there are two contributions to the absorption, represented here by the imaginary part of P_{ij} :

- (1) scattering of the existing quasiparticles,
- (2) breaking up of a Cooper pair with the consequent formation of two quasiparticles.

⁴⁴ P. L. Richards and M. Tinkham, Phys. Rev. **119**, 575 (1960).

⁴⁵ It is interesting to note that there is a tendency for the precursor to appear in metals that have an anisotropic gap, and hence it may be connected with the anisotropic character of the effective electron-electron interaction.

At very low temperatures, the number of existing quasiparticles is negligibly small and no scattering is possible. Absorption is then caused by the second mechanism and requires a certain minimum frequency. Since we are interested in this threshold behavior, the gap involved may be considered real and independent of quasiparticle energy. For the case of an isotropic gap, the absorption near the threshold has been calculated by previous investigators.⁴⁶⁻⁴⁸ In general, there are two features to be considered:

- (1) the value of the threshold energy,
- (2) the absorption line shape near the threshold.

Simple energy and momentum conservation arguments are sufficient to determine the threshold. Following Pokrovskii and Ryvkin,¹² we write for conservation of energy

$$\omega = E_p + E_{p-q}, \quad (7.21)$$

where

$$E_p = [\epsilon_p^2 + \Delta^2(\theta_p, \varphi_p)]^{1/2}, \quad (7.22)$$

$$E_{p-q} = [(\epsilon_p - \mathbf{v} \cdot \mathbf{q})^2 + \Delta^2(\theta_{p-q}, \varphi_{p-q})]^{1/2}. \quad (7.23)$$

Here ω , \mathbf{q} are the photon energy and momentum, and \mathbf{v} is the electron velocity. Since $p \gg q$, one may assume that $\theta_p \cong \theta_{p-q} \equiv \theta$, $\varphi_p \cong \varphi_{p-q} \equiv \varphi$, and solve Eq. (7.21), which yields two solutions

$$\epsilon_{p,1,2} = \frac{1}{2} \left\{ \mathbf{v} \cdot \mathbf{q} \pm \omega \left[\frac{\omega^2 - (\mathbf{v} \cdot \mathbf{q})^2 - 4\Delta^2(\theta, \varphi)}{\omega^2 - (\mathbf{v} \cdot \mathbf{q})^2} \right]^{1/2} \right\}. \quad (7.24)$$

Since ϵ_p must be real, the threshold frequency Ω is given by

$$\Omega^2 = \text{Min}[(\mathbf{v} \cdot \mathbf{q})^2 + 4\Delta^2(\theta, \varphi)]. \quad (7.25)$$

In order to find the (θ, φ) for which Ω is a minimum, we first write

$$\Delta(\theta, \varphi) = \Delta_0 + \Delta_1(\theta, \varphi), \quad (7.26)$$

where Δ_0 is an average value and Δ_1 includes all the anisotropy. We see that for

$$vq \gg \Delta_1(\theta, \varphi), \quad (7.27)$$

the minimum of Eq. (7.25) occurs when v is almost perpendicular to \mathbf{q} . In lead, $\Delta_1(\theta, \varphi)$ is of the order of 10% of Δ_0 , and assuming that the photon wave vectors of greatest importance are approximately equal to the reciprocal of the penetration depth, we have⁴⁴

$$\frac{vq}{\Delta_1} \cong \frac{vq}{0.1\Delta_0} \cong \frac{\xi}{0.1\delta} \cong 30. \quad (7.28)$$

⁴⁶ D. C. Mattis and J. Bardeen, Phys. Rev. **111**, 412 (1958).

⁴⁷ A. A. Abrikosov, L. P. Gorkov, and I. M. Khalatnikov, Zh. Eksperim. i Teor. Fiz. **35**, 265 (1958) [English transl.: Soviet Phys.—JETP **35**, 195 (1959)].

⁴⁸ D. J. Scalapino, J. R. Schrieffer and J. W. Wilkins (private communication and to be published) have calculated the absorption for isotropic lead with a complex, energy dependent gap. Near the threshold, their result coincides with that obtained in Refs. 46 and 47.

Pokrovskii failed to note that the criterion for a minimum to occur when \mathbf{v} is almost perpendicular to \mathbf{q} involves the anisotropic part of the gap and not the gap itself. Thus Eq. (7.27) is well satisfied in lead even though the condition for the extreme anomalous limit, i.e.,

$$\xi/\delta \gg 1 \quad (7.29)$$

is not well satisfied.

The imaginary part of P_{ij} is given by

$$\text{Im}P_{ij} \propto \int_{\text{AREA}} \int \frac{\sin\theta}{\rho_G(\theta, \varphi)} \langle \mathcal{P}_i | \mathbf{p} - \mathbf{q} \rangle \langle \mathbf{p} - \mathbf{q} | \mathcal{P}_j | \mathbf{p} \rangle \times \left\{ \frac{E_1 E_2 + \epsilon_p)_1 \epsilon_p)_2 - \Delta^2(\theta, \varphi)}{\epsilon_p)_1 E_2 - \epsilon_p)_2 E_1} \right\} d\theta d\varphi. \quad (7.30)$$

$\rho_G(\theta, \varphi)$ is the Gaussian curvature of the Fermi surface, \mathcal{P} is the momentum operator, and we have assumed that the matrix elements are independent of ϵ_p , for ϵ_p small. In lead, the band gaps are on the order of 1 eV, and hence for absorption near the threshold, i.e., $\hbar\omega = 0.027$ eV, we may ignore the interband parts of the matrix elements in Eq. (7.30), and assume that they are proportional to the product of components of the usual intraband velocities, $v_i v_j$.

In order to evaluate Eq. (7.30), we follow Pokrovskii and Ryykin. Two contributions are of importance, that of the area of integration and that of the coherence factor given by the bracketed expression of the equation. We use the expansions

$$\Delta(\theta, \varphi) = \Delta_m [1 + (a/2)(\theta - \theta') + (b/2)(\varphi - \varphi')^2], \quad (7.31)$$

and

$$\mathbf{v} \cdot \mathbf{q} = vq c(\theta - \theta'). \quad (7.32)$$

The locally orthogonal coordinates θ and φ are chosen so that the curve $\mathbf{v} \cdot \mathbf{q} = 0$ is described by $\theta = \theta'$ and the energy gap along the curve $\Delta(\theta', \varphi)$ takes minimum value Δ_m at the point (θ', φ') . Phase-space and energy-conservation arguments show that the region of integration is an ellipse with semiaxes,

$$l_1 = \left(\frac{2}{b} \right)^{1/2} \left(\frac{\omega}{\Omega} - 1 \right)^{1/2} \quad (7.33)$$

and

$$l_2 = \frac{2\sqrt{2}\Delta_m}{vqc} \left(\frac{\omega}{\Omega} - 1 \right)^{1/2}, \quad (7.34)$$

centered at the point $\varphi = \varphi'$, $\theta = \theta' - (2a\Delta_m^2/v^2q^2c^2)$. If b is nonzero, the area is proportional to $[(\omega/\Omega) - 1]$; if, however, $b = 0$, or is very small, the ellipse degenerates into a strip of width $2l_2$, running around the Fermi surface, whose area is proportional to $[(\omega/\Omega) - 1]^{1/2}$. The coherence factor, on the other hand, depends critically on the parameter a . A straightforward calculation shows that for a nonzero a , the leading term goes as $[(\omega/\Omega) - 1]^{-1/2}$; for $a = 0$, the leading term goes as

$[(\omega/\Omega) - 1]^{1/2}$. For $\omega > \Omega$, the leading term of the imaginary part of the polarization is then of the following form.

$$\begin{aligned} \text{Im}P_{ij} &\propto (a^2/b^{1/2}c^3)[(\omega/\Omega) - 1]^{1/2}, & a \neq 0, b \neq 0; \\ \text{Im}P_{ij} &\propto (1/b^{1/2}c)[(\omega/\Omega) - 1]^{3/2}, & a = 0, b \neq 0; \\ \text{Im}P_{ij} &\propto a^2/c^3, & a \neq 0, b = 0; \\ \text{Im}P_{ij} &\propto (1/c)[(\omega/\Omega) - 1], & a = 0, b = 0. \end{aligned} \quad (7.35)$$

The last case is the usual result for isotropic superconductors. The second case will be observed when light is incident in a direction perpendicular to a reflection plane of the crystal, e.g., the $\langle 100 \rangle$ and $\langle 110 \rangle$ directions in lead. When c is large, i.e., the angle between \mathbf{v} and \mathbf{q} changes rapidly as \mathbf{v} is moved off the line $\theta = \theta'$, only a small region of integration contributes and the absorption is reduced.

The use of Eqs. (7.31) and (7.32) in (7.25) gives an expression for the threshold frequency

$$\Omega = 2\Delta_m [1 - (a^2/2c^2)(\Delta_m/vq)^2]. \quad (7.36)$$

Since $(\Delta_m/vq)^2 \cong 0.1$, and, for most relevant portions of the Fermi surface, $c^2 > a^2$,

$$\Omega \cong 2\Delta_m. \quad (7.37)$$

One convenient experimentally observed quantity is the surface impedance tensor Z_{ij} given in a diagonalized form by

$$Z_{kk} = R_k + iX_k = \frac{E_k(0)}{\int_0^\infty J_k(z) dz} \propto i \left(\frac{1}{|\mathbf{P}|_k} \right)^t. \quad (7.38)$$

Here the index k refers to a set of Cartesian coordinates in the surface plane chosen to diagonalize the polarization tensor, and in the extreme anomalous limit

$$\begin{aligned} t &= \frac{1}{3} \quad \text{for } a = 0; \\ t &= \frac{1}{2} \quad \text{for } a \neq 0. \end{aligned}$$

The polarization is then of the form

$$P_{jk} = |P|_j \delta_{jk}, \quad (7.39)$$

where, in the general case, when $a \neq 0$, $b \neq 0$

$$\begin{aligned} |P|_k &= A_k & (\omega - \Omega) < 0, \\ |P|_k &= A_k + B_k(\omega - \Omega)^{1/2} i & (\omega - \Omega) > 0. \end{aligned} \quad (7.40)$$

A_k and B_k are real quantities whose variation with ω in the threshold region may be neglected.

An unpolarized beam measures some linear combination Z_{obs} of Z_{kk} . Expanding (7.38), one obtains

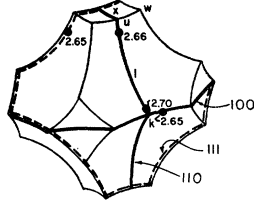
$$Z_{\text{obs}} = \beta i \quad (\omega - \Omega) < 0,$$

and

$$Z_{\text{obs}} = \alpha(\omega - \Omega)^{1/2} + \beta i \quad (\omega - \Omega) > 0, \quad (7.41)$$

where α and β are again real quantities which may be considered independent of ω in the threshold region. For

FIG. 19. The second-zone hole surface with the curves defined by $\mathbf{v} \cdot \mathbf{q} = 0$, for \mathbf{q} in the three main symmetry directions.



cases other than $a \neq 0$, $b \neq 0$, the real part of Z_{obs} has a functional dependence on $(\omega - \Omega)$ like that of P_{ij} in Eq. (7.35).

We return now to the specific case of lead. In order to find the values of the frequency at which the real part of the impedance becomes nonzero, we first located those curves on the Fermi surface on which $\mathbf{v} \cdot \mathbf{q} = 0$. In the free electron model, if the direction of \mathbf{q} is defined to be the polar axis, \mathbf{v} is perpendicular to \mathbf{q} on the equator.

On the actual Fermi surface, the relevant curves cannot be described as simply. Figure 19 schematically shows the curves on the second-zone hole surface on which $\mathbf{v} \cdot \mathbf{q} = 0$, for \mathbf{q} in each of the three main symmetry directions. The curves on the third-zone electron surface defined by $\mathbf{v} \cdot \mathbf{q} = 0$ are more difficult to determine. A complete analysis has been performed, but we confine ourselves here to the following remarks:

- (1) The quasiparticle velocity at the points r and q (see Fig. 10) is in a $\langle 110 \rangle$ -type direction, and hence perpendicular to any phonon wave vectors in a $\langle 110 \rangle$ plane, in particular those in the three principal symmetry directions.
- (2) The velocities on the line rtq (see Fig. 10) are perpendicular to a phonon wave vector in a $\langle 110 \rangle$ direction.

In order to find the threshold frequencies, we then located the points on the various curves where the gap is a relative minimum. For light propagation in *any* given direction, we expect to find, in general, several minima originating on different curves and/or different parts of the same curve. The various minima on the relevant curves of the second Brillouin zone surface are indicated in Fig. 19. Since the gap value at the point r on the third-zone surface is an absolute minimum, and since the velocity there satisfies the relevant condition, a threshold structure at 2.55 meV should be present for any \mathbf{q} in a $\langle 110 \rangle$ plane. In addition, the curve rtq contributes a threshold structure at 2.71 meV for \mathbf{q} in a $\langle 110 \rangle$ direction. Various other threshold structures are present between 2.60 and 2.65 meV for \mathbf{q} in any of the symmetry directions. Such structure would probably be difficult to resolve in any actual experiment.

C. Acoustic Attenuation

The BCS expression for the ratio of the acoustic attenuation in an isotropic superconductor with gap

Δ_{BCS} to that in a normal metal is given by

$$\alpha_S/\alpha_N = 2f(\Delta_{\text{BCS}}/kT), \quad (7.42)$$

where f is the Fermi function.

We use the results of Pokrovskii in order to interpret acoustic attenuation experiments in an anisotropic superconductor. To be sure, recent experiments^{49,50} have indicated that the attenuation in lead is amplitude dependent, and hence that the strong-coupling nature of the material may play an essential role—one not considered by Pokrovskii.¹¹ This possibility is, of course, a suitable subject for a future extensive investigation. Nevertheless, in order to make some semiquantitative experimental predictions, we quote Pokrovskii's expression

$$\alpha_S/\alpha_N \propto (T/T_c)^{1/2} \exp[-\Delta_m/kT]. \quad (7.43)$$

Here Δ_m is the minimum value of the gap on the curve defined by $\mathbf{v} \cdot \mathbf{q} = 0$, where \mathbf{q} is the momentum of the sound wave. We are thus concerned with the same curves on the Fermi surface which were of importance in the preceding section. Equation (7.43) holds when

$$\frac{v^2 \left(\frac{\Delta_m}{kT} \right)^{1/2}}{c^2} \exp \left[-\frac{(\Delta_m - \Delta_{am})}{kT} \right] \gg 1, \quad (7.44)$$

and

$$(\Delta_m/kT)^{3/2} c/v \ll 1, \quad (7.45)$$

where Δ_{am} is the absolute minimum gap on the Fermi surface, c is the velocity of sound in the material, and v is the Fermi velocity. In lead, $c/v = 10^{-3}$, and hence both of the above conditions are well satisfied in the region attained in experiments. The basic form given in Eq. (7.43) is independent of the actual shape of the Fermi surface which only affects the constant of proportionality. We note that Scalapino, Wada, and Swihart⁵¹ have solved Eqs. (3.11) and (3.12), suitably modified for finite temperatures, and shown that $\Delta(\Delta_{\text{BCS}})$ obeys the BCS temperature law. It is reasonable to assume that the anisotropic gap calculated from those equations has the same temperature dependence. The values of Δ_m that enter Eq. (7.43) for sound propagation in each of the three main symmetry directions are the same as those found in the last section. Because of the form of Eq. (7.43), only the lowest value of Δ_m for a given \mathbf{q} direction is observable at low temperatures. Since the absolute minimum value of the gap, 1.28 meV, appears for each of the symmetry directions, there is no way to distinguish between them. However, as the phonon propagation vector is tilted off the $\langle 110 \rangle$ plane, the smallest gap appearing should become larger than 1.28 meV. The rate of change of the minimum relevant gap depends on the detailed shape of the tubes near r (see Fig. 10).

⁴⁹ B. R. Tittmann and H. E. Bömmel, Phys. Rev. Letters **14**, 296 (1965).

⁵⁰ R. E. Love, R. W. Shaw, and W. A. Fate (to be published).

⁵¹ D. J. Scalapino, Y. Wada, and J. C. Swihart, Phys. Rev. Letters **14**, 102 (1965).

ACKNOWLEDGMENTS

I wish to thank: Dr. K. Maki and Dr. M. J. Zuckermann for interesting and informative discussions, Dr. J. R. Anderson for sending unpublished results on the band structure of lead, Dr. D. J. Scalapino for providing both the values of Δ and Z calculated by Dr. J. C. Swihart and the unpublished calculation referred to in Ref. 48. I am deeply grateful to Dr. L. M. Falicov for having suggested this problem. His patient instruction and guidance were of great value throughout the work.

This research was supported by both the National Aeronautics and Space Administration and the National

Science Foundation. In addition, it benefitted indirectly from the support to the Institute for the Study of Metals by the Advanced Research Projects Agency and the Office of Naval Research.

APPENDIX

We consider, as an example, the effect of a local minimum (Δ_m) of $\Delta(\theta, \varphi)$ on $N(E)$ and $dN(E)/dE$ for an anisotropic superconductor-normal metal junction at zero temperature. From Table IV and Eq. (7.7), we have

for $E < \Delta_m$,

$$\lim_{E \rightarrow \Delta_m^-} N(E) = C \int_0^E \frac{E}{(E^2 - x^2)^{1/2}} dx = \frac{1}{2} \pi C E, \quad (\text{A1})$$

$$\lim_{E \rightarrow \Delta_m^-} dN(E)/dE = \frac{1}{2} \pi C, \quad (\text{A2})$$

and for $E > \Delta_m$,

$$\lim_{E \rightarrow \Delta_m^+} N(E) = C \int_0^{\Delta_m} \frac{E dx}{(E^2 - x^2)^{1/2}} + (C+D) \int_{\Delta_m}^E \frac{E dx}{(E^2 - x^2)^{1/2}} = \frac{1}{2} \pi (C+D) E - DE \sin^{-1}(\Delta_m/E), \quad (\text{A3})$$

$$\lim_{E \rightarrow \Delta_m^+} \frac{dN(E)}{dE} = \frac{1}{2} \pi (C+D) + \frac{D}{\sqrt{2}(1 - \Delta_m/E)^{1/2}}. \quad (\text{A4})$$

Since the lower integration limit does not affect the results in any essential way, it is taken to be zero for simplicity.

We now consider the effect of Δ_m on the derivative of the tunneling current at zero temperature between two superconductors, one isotropic (1) and the second anisotropic (2). From (A1), (A3), and (7.3), we have

for $eV < \Delta_1 + \Delta_m$,

$$I_{<}(eV) = P \int_{-Q}^{-\Delta_1} N_1(E) N_2(E+eV) dE = P \int_{-Q}^{-\Delta_1} \frac{E}{(E^2 - \Delta_1^2)^{1/2}} \frac{1}{2} \pi C (E+eV) dE, \quad (\text{A5})$$

and for $eV > \Delta_1 + \Delta_m$,

$$I_{>}(eV) = P \int_{-Q}^{-\Delta_1} \frac{E}{(E^2 - \Delta_1^2)^{1/2}} \frac{1}{2} \pi C (E+eV) dE + P \int_{-\Delta_1}^{-\Delta_1 + \Delta_m} \frac{E}{(E^2 - \Delta_1^2)^{1/2}} D (E+eV) \left(\frac{1}{2} \pi - \sin^{-1} \frac{\Delta_m}{E+eV} \right) dE, \quad (\text{A6})$$

where Q is a lower integration limit which does not affect the results in any essential way. Subtraction, integration, and differentiation then yield

$$\begin{aligned} \lim_{eV \rightarrow \Delta_1 + \Delta_m} \frac{d}{dV} [I_{>}(eV) - I_{<}(eV)] &= \lim_{eV \rightarrow \Delta_1 + \Delta_m} \frac{d}{dV} P D \int_{-\Delta_1}^{-\Delta_1 + \Delta_m} \frac{E(E+eV)}{(E^2 - \Delta_1^2)^{1/2}} \left(\frac{1}{2} \pi - \sin^{-1} \frac{\Delta_m}{E+eV} \right) dE \\ &\cong \frac{1}{2} e P D \pi (\Delta_1 \Delta_m)^{1/2}. \end{aligned} \quad (\text{A7})$$